

## GALAXIES IN $N$ -BODY SIMULATIONS: OVERCOMING THE OVERMERGING PROBLEM

ANATOLY A. KLYPIN, STEFAN GOTTLÖBER<sup>1</sup>, AND ANDREY V. KRAVTSOV

Astronomy Department, New Mexico State University, Box 30001, Dept. 4500, Las Cruces, NM 88003-0001

ALEXEI M. KHOKHLOV

Laboratory for Computational Physics and Fluid Dynamics, Code 6404, Naval Research Laboratory,  
Washington, DC 20375

Astrophysical Journal, in press

### ABSTRACT

We present analysis of the evolution of dark matter halos in dense environments of groups and clusters in dissipationless cosmological simulations. The premature destruction of halos in such environments, known as the *overmerging*, reduces the predictive power of  $N$ -body simulations and makes difficult any comparison between models and observations. We analyze the possible processes that cause the overmerging and assess the extent to which this problem can be cured with current computer resources and codes. Using both analytic estimates and high resolution numerical simulations, we argue that the overmerging is mainly due to the lack of numerical resolution. We find that the force and mass resolution required for a simulated halo to survive in galaxy groups and clusters is extremely high and was almost never reached before:  $\sim 1 - 3$  kpc and  $10^8 - 10^9 M_\odot$ , respectively. We use the high-resolution Adaptive Refinement Tree (ART)  $N$ -body code to run cosmological simulations with the particle mass of  $\approx 2 \times 10^8 h^{-1} M_\odot$  and the spatial resolution of  $\approx 1 - 2 h^{-1}$  kpc, and show that in these simulations the halos do survive in regions that would appear overmerged with lower force resolution. Nevertheless, the halo identification in very dense environments remains a challenge even with the resolution this high. We present two new halo finding algorithms developed to identify both isolated and satellite halos that are stable (existed at previous moments) and gravitationally bound.

To illustrate the use of the satellite halos that survive the overmerging, we present a series of halo statistics, that can be compared with those of observed galaxies. Particularly, we find that, on average, halos in groups have the same velocity dispersion as the dark matter particles, i.e. do not exhibit significant velocity bias. The small-scale (100 kpc – 1 Mpc) halo correlation function in both models is well described by the power law  $\xi \propto r^{-1.7}$  and is in good agreement with observations. It is slightly antibiased ( $b \approx 0.7 - 0.9$ ) relative to the dark matter. To test other galaxy statistics, we use the maximum of halo rotation velocity and the Tully-Fisher relation to assign the luminosity to the halos. For two cosmological models, a flat model with the cosmological constant and  $\Omega_0 = 1 - \Omega_\Lambda = 0.3$ ,  $h = 0.7$ , and a model with a mixture of cold and hot dark matter and  $\Omega_0 = 1.0$ ,  $\Omega_\nu = 0.2$ ,  $h = 0.5$ , we construct the luminosity functions and evaluate mass-to-light ratios in groups. Both models produce luminosity functions and the mass-to-light ratios ( $\sim 200 - 400$ ) that are in a reasonable agreement with observations. The latter implies that the mass-to-light ratio in galaxy groups (at least for  $M_{vir} \lesssim 3 \times 10^{13} h^{-1} M_\odot$  analyzed here) is not a good indicator of  $\Omega_0$ .

*Subject headings:* cosmology: theory – large-scale structure of universe – methods: numerical

### 1. INTRODUCTION

It is generally believed that the dark matter (DM) constitutes a large fraction of the mass in the Universe and thus significantly affects, and on some scales dominates, the process of galaxy formation. Observational evidence for large fractions of DM in galaxies, groups, and galaxy clusters ranges from flat rotational curves of spiral (e.g., Faber & Gallagher, 1979; Rubin et al. 1985; Persic, Salucci, & Stel 1996; Courteau & Rix, 1997) and X-ray emission and mass-to-light ratios of elliptical (Forman et al. 1985; Rix 1997; Brighenti & Mathews 1997) galaxies to the baryon fractions in clusters of galaxies (White et al. 1993; Evrard 1997). For galaxies, the extent of the DM halos estimated using satellite dynamics, is  $\sim 0.2 - 0.5 h^{-1}$

Mpc<sup>2</sup> (Zaritsky & White 1994; Carignan et al. 1997). A convincing evidence for substantial amounts of dark matter even in the very inner regions of galaxies comes from the recent HI studies of the dwarf and low surface brightness (LSB) galaxies. The observed amounts of stars and gas in some of these galaxies can account for less than 10% of the observed rotational velocities at the last measured point of the rotation curves. (e.g., Carignan & Freeman 1988; Martimbeau, Carignan, & Roy 1994; de Blok & McGaugh 1997).

If the observed galaxies have large DM halos, then  $N$ -body simulations can, in principle, be used to predict distribution of the dark matter component, to associate the simulated DM halos with galaxies, and to predict the bulk

<sup>1</sup>On leave from Astrophysikalisches Institut Potsdam (AIP), An der Sternwarte, 16, D-14482, Potsdam, Germany

<sup>2</sup>Throughout this paper we assume that the present-day Hubble constant is  $H_0 = 100h$  kms<sup>-1</sup>Mpc<sup>-1</sup>.

properties of these galaxies such as position, mass, and size. One should be able then to make predictions about spatial distribution and motion of these simulated galaxies and compare these predictions with corresponding observations. Unfortunately, the dissipationless numerical simulations have been consistently failing to produce galaxy-size dark matter halos in dense environments typical for galaxy groups and clusters (e.g., White 1976; van Kampen 1995; Summers, Davis, & Evrard 1995; Moore, Katz, & Lake 1996). This apparent absence of substructure in the virialized objects, known as *the overmerging problem*, reflects the fact that simulated galaxies seem to merge much more efficiently in comparison with real galaxies in groups and clusters. In the central regions of a cluster ( $\sim 500$  kpc), the “overmerging” erases not only large-scale substructure, but also any trace of small halos that could be associated with “galaxies”<sup>3</sup>, leaving a smooth giant lump of dark matter.

The overmerging problem was traditionally explained by the lack of dissipation in  $N$ -body simulations (e.g., Katz, Hernquist & Weinberg 1992; Summers et al. 1995). Indeed, the DM halos are much larger than baryonic extent of the galaxies due to the dissipational nature of the latter. The radiative cooling, for example, allows baryonic component to sink into the center of the DM halo where it forms a compact, tightly bound object. In dense environments the large DM halo can be easily stripped by the tidal field of a galaxy cluster or group, whereas the more compact and denser gas clump may survive (Summers et al. 1995). Although it is clear that to produce a realistic galaxy we need to include the energy dissipation by baryons, it is not clear whether the dissipation is vital for the halo survival in a cluster.

Two arguments can be presented against the traditional explanation for the overmerging. First, if the dissipation helps galaxies to survive in clusters, then galaxies should be dominated by baryons at all scales within their visible extent. Most of the observed galaxies, however, appear to have a substantial fraction of DM inside their optical radius (e.g., Persic et al. 1996). The survival of a galaxy dominated at its optical radius by the dark matter will depend mostly on the dark matter, not on the baryons. The DM dominated dwarfs must have been tidally disrupted, but dwarf galaxies are observed in clusters (e.g. Smith, Driver, & Phillipps 1997; Lopez-Cruz et al. 1997). Second, as we argue in this paper, even in the absence of the baryons DM halos are dense enough to survive inside clusters and to be identified, provided that simulations have sufficient resolution *in both* mass and force (similar conclusion was reached by Moore et al. 1996).

The main goal of this paper is to demonstrate that with a sufficient computational effort the overmerging problem can be tamed (at least to some extent) even in the purely dissipationless simulations. The computational costs are higher than cost of an average cosmological  $N$ -body simulation. However, they may be considerably lower than computational expense of the corresponding  $N$ -body+hydro simulations. This especially true in the case

of large-volume ( $\sim 50 - 100h^{-1}$  Mpc) simulations required to quantify the statistical properties of the “galactic” populations such as correlation function, pairwise velocity dispersions etc. To understand how the problem should be dealt with, it is important to understand what processes lead to the overmerging.

Several recent studies have addressed this question from different viewpoints and using different numerical and analytical techniques. Thus, for example, van Kampen (1995) studied formation of galaxy clusters in purely dissipationless simulations and concluded that two-body relaxation and tidal disruption are primarily responsible for the overmerging. He found, however, that the two-body effects are important only for the smallest halos ( $\lesssim 30$  DM particles), in quantitative agreement with experiments of Moore et al. (1996). The latter study addressed also effects of particle-halo and halo-halo heating on the survival of DM halos. The authors concluded that particle-halo heating does not pose a problem as long as DM particle mass is  $\lesssim 10^{10}M_{\odot}$ , but halo-halo heating may be important if force resolution is not adequate ( $\gtrsim 10$ kpc). The general conclusion of Moore et al. is that the overmerging problem is due mainly to tidal heating by the cluster and halo-halo heating, both effects being enhanced by poor force resolution. They note also that these effects depend crucially on the density structure of DM halos.

The density profile of dark matter halos in the CDM models is now known reasonably well. Navarro, Frenk & White (1995, 1996, 1997, hereafter NFW) gave an analytical fit that describes with a reasonable accuracy the density profiles of DM halos formed in the standard cold dark matter scenario over large range of scales and masses. The analytical form of the density profile advocated by NFW, allows one to estimate tidal effects and effects of dynamical friction analytically. We present these estimates in §2.

Two recent numerical studies (Tormen, Diaferio & Syer 1998; and Ghigna et al. 1998) present evidence that higher resolution significantly alleviates the overmerging problem in dissipationless simulations. Both studies conclude that many halos survive for a long time after falling onto a large halo, although overmerging problem persists to a certain degree in the central dense region of the large cluster-size halo. Tormen et al. also point out that there are real physical processes which would lead to the erase of substructure even in the ideal very high-resolution simulation. Namely, the dynamical friction drives massive satellites to the cluster core where they get tidally stripped and quickly disrupted. This effect is, of course, real and should be distinguished from artificial overmerging caused by insufficient numerical resolution. We will address these issues in §2.

Two goals of the study presented in this paper are 1) to make an approximate estimates of the effects leading to the overmerging for the halos with the NFW density distribution; and 2) to demonstrate that dissipationless simulations with sufficiently high resolution in force and mass are affected by the overmerging to a considerably lesser degree. In other words, we present an attempt to

<sup>3</sup>The term “galaxy” traditionally refers to luminous observed objects (i.e. to clumps of stars and gas, not the DM), which, possibly, are embedded in a considerably larger DM “halo”. The term “halo”, however, is rather general. We can use this term to indicate a galaxy cluster, group, or a galaxy-size halo. In some cases, we want to make a clear distinction between these. We will thus use terms “simulated galaxies” or “galaxy-size halo” to indicate the DM halos formed in the simulations which could be associated with places where luminous baryons could reside.

estimate to which extent the overmerging problem can be solved with numerical resolution that can be achieved with current codes and computational resources. The goal is worthwhile. If the problem can be minimized at a computational cost that is not prohibitive, the dissipationless simulations can be used for a direct study of the statistical properties of “galaxies”. This may include studies of their spatial distribution, velocity field, environmental effects etc. This may allow us to make a step towards solution of the long-standing and particularly important issue of the galactic bias.

The overall plan of the paper is as follows. In §2 we discuss the numerical and physical effects which may lead to the erasure of substructure inside the dense massive halos. Specifically, we present analytical estimates for tidal disruption of dark matter halos and effects of dynamical friction assuming that halos are described by the NFW density profile. We use these calculations to make a rough estimate of what resolution would be required to minimize the overmerging. Numerical simulations and cosmological models are discussed in §3. In §4 we discuss difficulties associated with identification of dark matter halos in very dense regions. We describe two new halo finding algorithms developed to handle the halos in such environments. In §5 we present results of high-resolution dissipationless simulations, illustrate the performance of the new halo finding algorithms and discuss the degree to which the simulations are affected by the overmerging. Our conclusions are illustrated using well-known statistics such as two-point correlation function, velocity bias, luminosity function and  $(M/L)$  ratio. The conclusions are summarized in §6.

## 2. SURVIVAL OF HALOS IN CLUSTERS

### 2.1. Numerical effects vs. physical effects

As was noted in the introduction, there is a number of processes potentially contributing to the erasure of substructure in clusters and groups (van Kampen 1995; Moore et al. 1996). Some of these processes are due to numerical limitations of a simulation, while others are real physical effects.

The major effects caused by numerical limitations are *particle evaporation* due to the two-body relaxation (e.g., Carlberg 1994; van Kampen 1995; Moore et al. 1996), *particle-halo heating* (Carlberg 1994; Moore et al. 1996), and *premature tidal disruption* due to an insufficient force resolution. The two-body evaporation in an  $N$ -body system is a well-understood process (e.g., Binney & Tremaine 1987). However, it was shown (van Kampen 1995; Moore et al. 1996) that the two-body evaporation is important only for the halos with  $\lesssim 30$  particles. Thus, if a simulation has a particle mass of  $\lesssim 10^9 h^{-1} M_\odot$ , this effect is not important for halos in the mass range of interest ( $\gtrsim 10^{11} h^{-1} M_\odot$ ). It may become important, however, if halo loses most of its mass due to the tidal stripping. The particle-halo heating was suggested by Carlberg (1994) as an explanation for overmerging in his simulation. However, Moore et al. (1996) showed that the time-scale for this process is large for typical numerical parameters. Finally, gravitational softening,  $r_{soft}$ , imposed in an  $N$ -body simulation usually leads to a constant density core  $r_c \approx r_{soft}$  in the halo center. Poor force resolution may,

thus, result in halos with artificially large cores which will be tidally disrupted faster than if they would have a more compact density distribution.

The real physical processes which may lead to the erasure of substructure include *dynamical friction*, *tidal stripping*, and *halo-halo heating*. The dynamical friction drives DM halos towards the high-density cluster center where they get tidally stripped and merge with the central massive object. Dynamical friction can be important for some halos and is probably responsible for the presence of massive central cD galaxies in observed clusters (e.g., Merritt 1985). The importance of dynamical friction for each particular halo will depend on the halo mass and details of its orbit. We will estimate these dependencies in §2.4. Tidal stripping occurs simply because at some distance from the center the tidal force from a cluster is stronger than gravitational force of a parent halo and particles beyond this radius become unbound from a halo and dissolve in the ambient diffuse medium. This effect will be discussed in the next section. Finally, Moore et al. (1996) argued that heating due to the close passages of DM halos on their orbits may lead to significant mass losses. Their estimate, however, was based on experiment in which cluster is static. In real clusters only a few halos will be present for its entire lifetime, the bulk of the halos being accreted over period of the cluster evolution. This process is probably less important than the more efficient tidal stripping.

Numerical and physical effects are, of course, closely related. Tidal force of the cluster and close encounters of individual dark halos result in effective stripping of the peripheral parts of the halos. This is a real physical effect. But after the stripping is done, two-body relaxation can become artificially short and can result in evaporation of halos if the number of particles in a halo is too small. Due to the dynamical friction halos tend to spiral down towards the center of the cluster where they merge with the central halo. This is a real effect. But it can be exacerbated by artificially high energy dissipation in hydrodynamical simulations resulting in too compact halos.

It is clear that physical processes will operate and will tend to erase substructure even in an ideal simulations of infinite resolution. The numerical effects, on the other hand, can be cured by improving the spatial and mass resolution of the simulations and/or by inclusion of additional physics (e.g., missing gas dissipation). It is the numerical effects that we will focus on in this paper. Throughout the rest of the paper, we will be using the term “overmerging problem” only for processes related to the numerical effects, which appear due to the lack of resolution or due to missing physical effects.

### 2.2. Tidal disruption of halos: analytical estimates

The main reason for the erasure of the substructure in clusters is the tidal interaction of individual halos with the cluster potential. This can be now estimated reliably, without assuming that halos are isothermal spheres or have King profiles, as was typically the case in the past (Moore et al. 1996). The density profiles of dark matter halos in the CDM models is now known reasonably well for a large range of masses and for a variety of cosmological models (NFW). Below we give analytic estimates for various halo properties in the standard  $\Omega = 1$  CDM model. The low-density flat CDM model with cosmolog-

ical constant ( $\Lambda$ CDM; e.g., Carrol, Press & Turner 1992) model predicts similar profiles, if the the overdensity of a collapsed object is adjusted properly to take into account the change in  $\Omega$  (Lahav et al. 1991; Eke et al. 1996).

The NFW density profile is given by

$$\rho(r) = \frac{\rho_0 r_s^3}{r(r+r_s)^2}, \quad M(r) = M_{\text{vir}} \cdot \frac{f(x)}{f(C)}, \quad (1)$$

$$f(x) \equiv \ln(1+x) - \frac{x}{1+x}, \quad x \equiv \frac{r}{r_s}.$$

where  $r_s$  and  $\rho_0$  are the characteristic radius and density of the halo,  $M_{\text{vir}}$  is the virial mass,  $r_{\text{vir}}$  is the virial radius, and  $C$  is the concentration for a halo defined as follows:

$$C \equiv \frac{r_{\text{vir}}}{r_s},$$

$$r_{\text{vir}}(M_{\text{vir}}) = 443 h^{-1} \text{kpc} \left( \frac{M_{\text{vir}}/10^{11} h^{-1} M_{\odot}}{\Omega_0 \delta_{\text{th}}} \right)^{1/3}, \quad (2)$$

$$M_{\text{vir}} \equiv \frac{4\pi}{3} \rho_{\text{cr}} \Omega_0 \delta_{\text{th}} r_{\text{vir}}^3.$$

Here,  $\rho_{\text{cr}}$  is the critical density of the Universe and  $\delta_{\text{th}}$  is the overdensity ( $\delta\rho/\rho_{\text{matter}}$ ) of a collapsed object according to the top-hat model of spherical collapse. For the CDM model  $\delta_{\text{th}} \approx 200$ . Note that our definition of  $r_{\text{vir}}$  differs from that used by NFW, who use  $\delta_{\text{th}} = 200$  for all cosmological models. We use values predicted by the top-hat model which gives, for example,  $\delta_{\text{th}} \approx 340$  for the  $\Lambda$ CDM model with  $\Omega_0 = 0.3$ .

The concentration  $C$  is a function of mass  $M_{\text{vir}}$ . In the case of the CDM model

$$C \approx 124 (M_{\text{vir}}/1h^{-1} M_{\odot})^{-0.084} \quad (3)$$

Typical values for the concentration  $C$  range from  $C \approx 12$  for  $M_{\text{vir}} = 10^{12} h^{-1} M_{\odot}$  to  $C \approx 7$  for  $M_{\text{vir}} = 10^{15} h^{-1} M_{\odot}$  (NFW). Using these definitions we can write mass  $M(r)$ , orbital frequency  $\omega(r)$ , and gravitational potential  $\phi(r)$ :

$$\omega^2(r) = \frac{GM}{r^3} = \frac{GM_{\text{vir}}}{r_s^3 f(C)} \cdot \frac{f(x)}{x^3},$$

$$\phi(r) = -\frac{GM_{\text{vir}}}{r_s f(C)} \cdot \frac{f(x) + \frac{x}{1+x}}{x}. \quad (4)$$

In some cases it is more convenient to define properties of halos by using maximum rotational velocity  $V_{\text{max}} = \sqrt{(GM/r)|_{\text{max}}}$ , halo parameter which is probably most easily related to an observable quantity, instead of the concentration  $C$  or the virial mass  $M_{\text{vir}}$ . For profile Eq.(1) the maximum of the rotational velocity occurs at  $r_{\text{max}} \approx 2r_s$ . This gives

$$V_{\text{max}}^2 = \frac{GM_{\text{vir}}}{r_s} \cdot \frac{f(2)}{2f(C)}, \quad f(2) \approx 0.432$$

$$M(r) = \frac{r_s V_{\text{max}}^2}{G} \cdot \frac{2f(x)}{f(2)}, \quad \omega^2(r) = \frac{V_{\text{max}}^2}{r_s^2} \cdot \frac{2f(x)}{x^3 f(2)}, \quad (5)$$

$$V_{\text{esc}}^2 = -2\phi(r) = 4V_{\text{max}}^2 \frac{\ln(1+x)}{xf(2)},$$

where  $V_{\text{esc}}$  is the escape velocity at the distance  $r$  from the cluster center.

The tidal radius,  $r_t$ , of a small halo with mass  $m$  and maximum rotational velocity  $v_{\text{max}}$  moving at a radius  $R$  from the center of a large halo with mass  $M(R)$  and  $V_{\text{max}}$ , is the minimum of two radii: (1) a radius at which the gravity force of the small halo  $F_{\text{grav}}$  is equal to the tidal force of the large halo  $F_{\text{tide}}$ , and (2) a radius defined by the resonances between the force the small halo exerts on the particle and the tidal force by the large halo. If  $r$  is the distance of a particle from the center of the small halo, then the condition  $F_{\text{grav}}(r) = F_{\text{tide}}(r; R)$  gives an equation for the tidal radius  $r_t$ :

$$\left(\frac{R}{r_t}\right)^3 \frac{m(r_t)}{M(R)} = 2 - \frac{R}{M} \frac{\partial M}{\partial R},$$

$$\frac{f(x_r)}{f(x_R)} = \left(\frac{x_r}{x_R}\right)^3 \left(\frac{r_s V_{\text{max}}}{R_s v_{\text{max}}}\right)^2 \left(2 - \frac{x_R^2}{(1+x_R)^2 f(x_R)}\right), \quad (6)$$

where  $x_r \equiv r_t/r_s$  and  $x_R \equiv R/R_s$ . The last equation can be solved numerically.

It was argued (e.g., Weinberg 1994ab, 1997) that effective tidal stripping can occur at smaller radius defined by resonances between the force the small halo exerts on the particle and the tidal force by the large halo. We assume that stripping mainly happens at primary resonance  $\omega(r)|_{\text{small}} = \omega(R)|_{\text{large}}$ . This leads to the following equation for the tidal radius:

$$\frac{f(x_r)}{f(x_R)} = \left(\frac{x_r}{x_R}\right)^3 \left(\frac{r_s V_{\text{max}}}{R_s v_{\text{max}}}\right)^2, \quad (7)$$

We take the smaller of the two estimates of  $r_t$ . For  $x_R > 2.2$  the tidal radius is defined by the equal force condition. At smaller distances the orbital-internal resonance defines the tidal radius.

Figure 1 shows tidal radius and mass within the tidal radius for halos at a given distance from the center of a group of galaxies with different masses. In this figure the mass of a dark halo, indicated next to each curve, is the virial mass of the unstripped halo, i.e. mass *before* the halo entered the cluster. As the distance from the cluster center decreases, the tidal radius of the halo and the mass within the tidal radius decrease accordingly. Even at large distances from the cluster center ( $R > 200h^{-1}\text{kpc}$ ) the halo radius changes significantly. For example, a halo with  $M_{\text{vir}} = 10^{12} h^{-1} M_{\odot}$  and  $r_{\text{vir}} = 163h^{-1}\text{kpc}$  at  $R = 200h^{-1}\text{kpc}$  from the center of  $10^{13} h^{-1} M_{\odot}$  group lost only 20% of its original mass, but its radius decreased by a factor of two. The mass inside the tidal radius  $m(r_t)$  changes with  $R$  much slower  $m \propto R^{0.3-0.5}$  than it would for the isothermal distribution for which we expect  $m \propto R$ . This is because the halos with profile Eq.(1) are more centrally concentrated  $\rho_{\text{halo}} \propto R^{-3}$  than isothermal halos ( $\rho_{\text{iso}} \propto R^{-2}$ ). Note that the central cusp in Eq.(1) is not important for survival of halos at large distances:  $r_s$  is smaller than the tidal radius  $r_t$ . At smaller distances ( $R \lesssim 2.2R_s$ ) mass within the tidal radius decreases faster ( $m \propto R$ ) and the orbital-internal resonance defines the tidal stripping. It is likely that we overestimate the effect of tidal destruction at these distances as compared to galaxies in real clusters because the tidal radius is small  $\sim 10h^{-1}\text{kpc}$  and the baryonic component cannot be neglected. At the same time, whether halos survive or not,

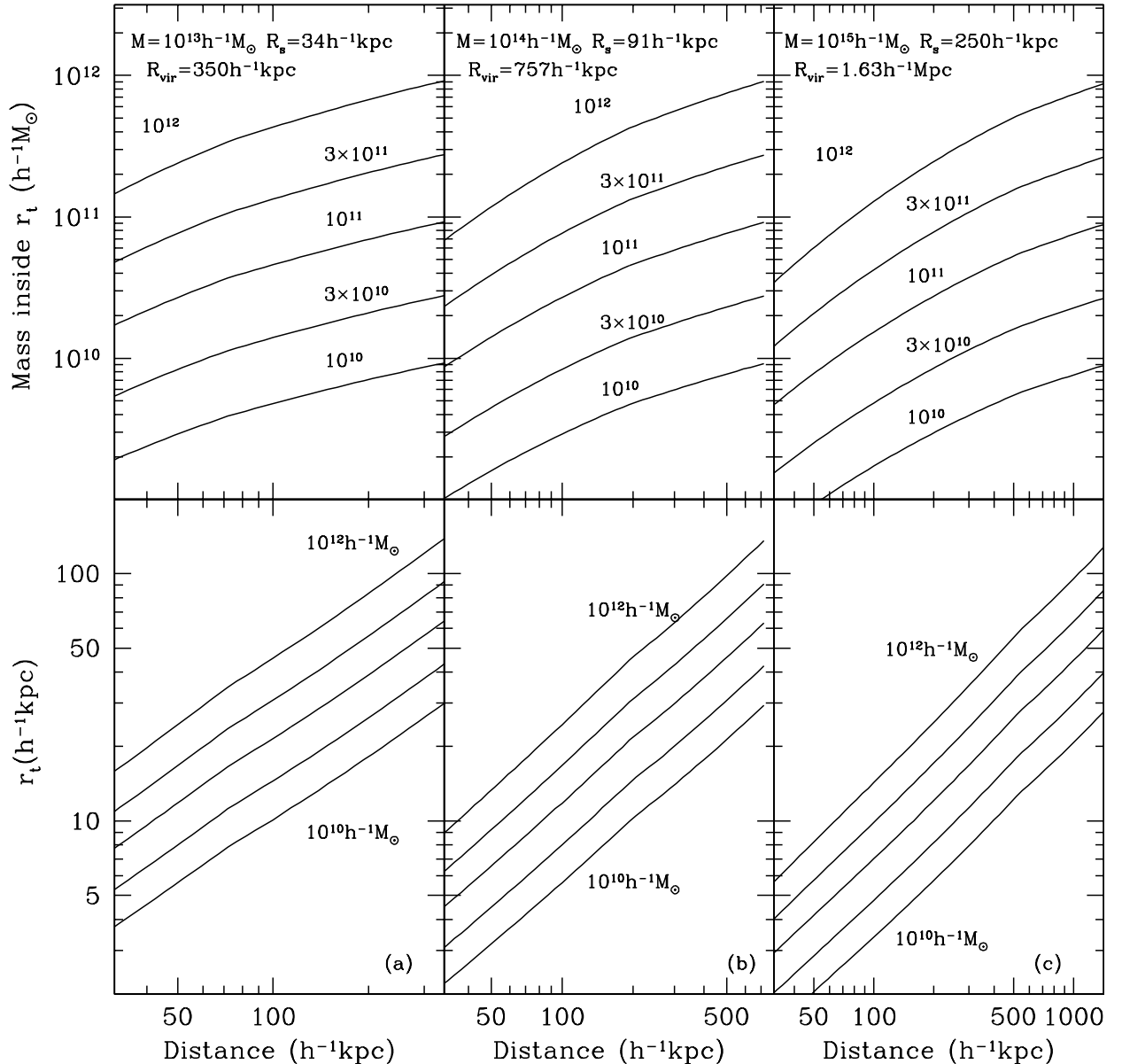


FIG. 1.— Tidal radii (bottom row) and masses within the tidal radius (upper row) for halos at a given distance from the center of a galaxy cluster of mass  $10^{13}h^{-1}M_{\odot}$  (a),  $10^{14}h^{-1}M_{\odot}$  (b), and  $10^{15}h^{-1}M_{\odot}$  (c). The density profiles for both the clusters and the halos are given by Eq.(1) with an appropriate concentration  $C(M)$ . In the figures the mass of a dark halo, indicated next to each curve, is the mass  $M_{\text{vir}}$  of the halo *before* tidal stripping, when the halo was outside the cluster virial radius.

they already have lost a very large fraction of their mass ( $\sim 90\%$ , exact number depends on parameters of the halo) when they get to  $R \lesssim R_s$ .

### 2.3. Effects of energy dissipation by baryons

Baryonic matter can loose energy by emitting radiation. This dissipation allows baryons to sink onto the centers of halos and produce a dense central region inside parent dark matter halo. Because a denser halo is more resistant to the tidal disruption, baryon dissipation clearly helps galaxies to survive in clusters. We consider two effects due to the energy dissipation. (i) The shape of the density profile in the central part of the halo changes without changing

much overall structure of the halo. (ii) Global parameters of the halo (such as its characteristic radius  $R_s$  and maximum rotational velocity  $V_{\text{max}}$ ) change in reaction to the motion of baryons into the center. Another possible effect is orbit circularization due to formation of rotationally supported baryonic disk. The effect of this last process, however, is difficult to estimate, but it likely affects only baryons. Below we discuss the first two effects.

(i) *The shape of the density profile in the halo center.* The main question here is how much our estimates of the tidal radius would change if we assumed a steeper central cusp.

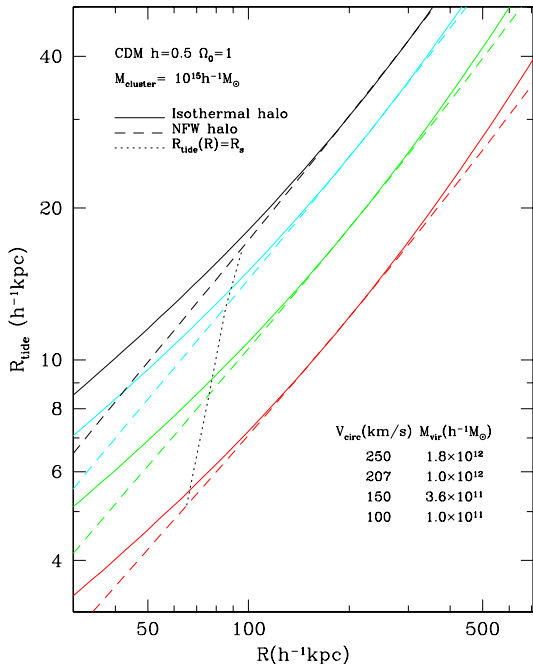


FIG. 2.— Tidal radii of halos of different masses and circular velocities inside a cluster of virial mass  $10^{15}h^{-1}M_{\odot}$ . Isothermal halos (solid curves) have larger tidal radii as compared with the NFW halos (dashed curves), which means that isothermal halos are more stable. Both isothermal and NFW halos have the same maximum circular velocity. The dotted curve shows distance at which the tidal radius is equal to the characteristic radius  $R_s$ . On the left from the curve the halos are tidally destroyed no matter what resolution is used. While the energy dissipation and subsequent baryonic infall increase the tidal radius, realistic dissipation is hardly a dramatic effect for halos.

To get an estimate of the effect, we assume that sinking of the baryons to the halo center produces flat rotation curve:  $V_c = \text{constant}$ ,  $\rho \propto r^{-2}$ . For simplicity, the rotational velocity is assumed to be equal to the maximum of the circular velocity of the DM halo before the dissipation. Figure 2 shows tidal radii of halos of different masses and circular velocities inside a cluster of mass  $10^{15}h^{-1}M_{\odot}$ . Isothermal halos have larger tidal radii, which means that they are more stable. Nevertheless, the difference with the NFW halos is very small at distances from cluster center larger than  $\sim 50h^{-1}\text{kpc}$ . Even at  $(30 - 50)h^{-1}\text{kpc}$  the difference is only 10%-20%. The dotted curve in this plot shows the distance at which the tidal radius is equal to the characteristic radius  $R_s$  of the satellite halos. At this distance the tidal radius of the isothermal halo is  $\lesssim 5\%$  larger than tidal radius of the NFW halos. Our  $N$ -body simulations presented in the next section indicate that halos which come that close to the center of a cluster will be tidally destroyed regardless of what resolution is used. They may leave a very small leftover, which, even if present, is so small that it cannot represent a galaxy. Thus, the change in the shape of the central density profile cannot significantly affect survival of halos inside clusters.

(ii) *Increase of the central density due to dissipation.* The next question is what effect for halo survival can have

possible increase of the central density (and hence maximum rotational velocity) due to the baryonic dissipation. Again, we assume that the halo after the dissipation has a flat rotation curve and, thus, its tidal radius can be roughly estimated using isothermal density profile. In Figure 2 the halo “moves” from the NFW curve (dashed line) to a higher isothermal curve (solid line). For example, a DM halo with the virial mass of  $10^{11}h^{-1}M_{\odot}$  with tidal radius of  $7h^{-1}\text{kpc}$  at  $100h^{-1}\text{kpc}$  from the cluster center can increase its tidal radius to  $10h^{-1}\text{kpc}$ , if its circular velocity increases from  $100\text{ km s}^{-1}$  to  $150\text{ km s}^{-1}$ . This may save the halo from the tidal destruction because its tidal radius is now about twice larger than its  $R_s$ . Unfortunately, there are limits on the increase of the rotational velocity. The gas possesses non-zero angular momentum, characterized by the dimensionless spin parameter  $\lambda$  (Binney & Tremaine 1987) and sooner or later becomes rotationally supported. For a typical value of  $\lambda = 0.05$ , the adiabatical infall model (e.g., Mo, Mao, & White 1998) predicts an increase of the maximum rotational velocity of  $V_{\text{cdisk}}/V_{\text{chalo}} = 1.3$ . (We use eqs. 33-34 in Mo, Mao, & White with the fraction of mass in disk  $m_d = 0.05$ ; a correction is made to convert from  $V_{200}$  to  $V_{\text{max}}$ ). Using a different approach to treat the baryonic infall, Avila-Reese, Firmani, & Hernandez (1998) arrive at the same correction: rotational velocity increases by a factor 1.3-1.4 for typical halo parameters. Figure 2 shows that such increase would correspond to  $\sim 20 - 40\%$  increase in the tidal radius. While the energy dissipation and subsequent baryonic infall increase the tidal radius, it is hardly a dramatic effect for realistic halos.

#### 2.4. Tidal disruption of halos: simple numerical simulations

Up to this point we have treated the tidal stripping in a rather simplified way. Such simplified treatment is useful, because it gives a rough approximation for a complicated process. In reality (even within the framework of dark matter dynamics), the situation is more complicated. This is especially true for halos that lose a significant fraction of mass, in which case stability of the halos against the two-body relaxation is an issue. When a halo loses mass, the mass is lost from peripheral parts. If the trajectories of particles are not circular (which is typically the case), the central region of the halo will start to “feel” the loss on a dynamical time-scale. Some of particles leave the center and are not replaced by tidally-stripped particles; this decreases the central density and leads to the expansion of the halo and to further loss of mass. The cycle may repeat, destroying eventually the entire halo. Whether this process leads to halo destruction or not depends on the orbit of the halo and its tidal radius.

In order to study the tidal stripping in a more realistic way, we run a set of small  $N$ -body simulations in which a halo of a few thousand self-gravitating particles moves in a rigid potential of a cluster. The cluster of the virial mass  $2 \times 10^{14}h^{-1}M_{\odot}$ , a typical cluster mass for large-scale simulations presented later in the paper, is assumed to have the NFW density profile eq.(1). To be consistent with our large simulations, we also use a  $\Lambda$ CDM cosmological model with the following parameters:  $\Omega_0 = 1 - \Omega_{\Lambda} = 0.3$ ,  $h = 0.7$ ,  $\sigma_8 = 1.0$ . The halo mass is chosen to be  $10^{12}h^{-1}M_{\odot}$ . This halo has the characteristic radius of  $R_s = 19.5h^{-1}\text{kpc}$  and the maximum circular velocity of  $190\text{ km s}^{-1}$ .

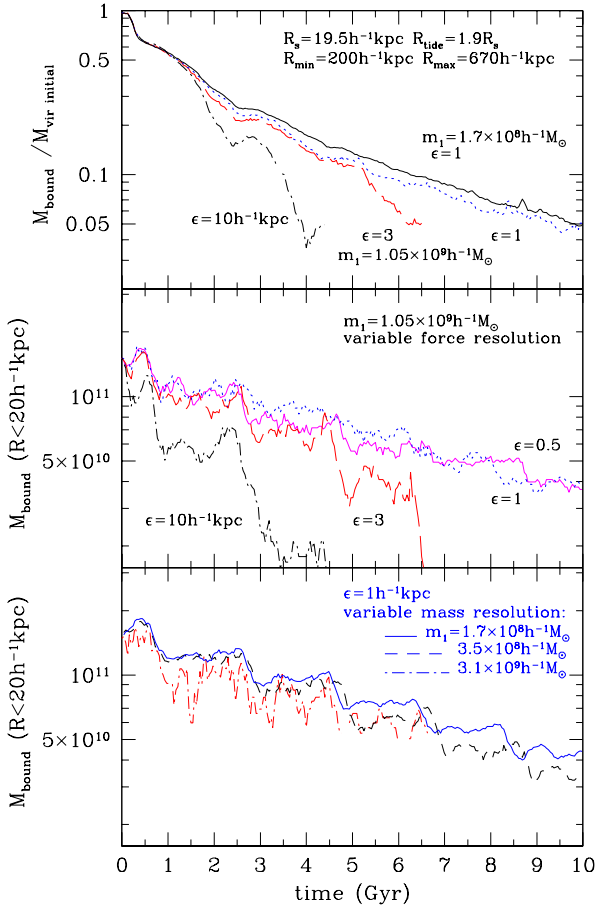


FIG. 3.— The evolution of the total bound mass (top panel) and the bound mass inside central  $20h^{-1}\text{kpc}$  radius (middle and bottom panels) for a halo with initial mass  $10^{12}h^{-1}M_{\odot}$  moving inside a cluster of virial mass  $2 \times 10^{14}h^{-1}M_{\odot}$ . Different curves correspond to different force and/or mass resolutions used in the experiment (each curve is marked with corresponding resolution). Both the cluster and (initially) the halo have the NFW density profiles. The simulations were done with different mass  $m_1$  and force  $\epsilon$  resolution. The halo loses 95% of its mass, but given sufficient resolution it survives for more than 10Gyr.

Within the radius of  $R_{200} = 163h^{-1}\text{kpc}$  the halo has overdensity 200 relative to the critical density of the Universe. At the initial moment the particles of the halo were distributed inside  $R_{200}$  in 100 equally spaced spherical shells in such a way that the density profile obeys eq.(1). Eq.(10) was used to find one dimensional velocity dispersion for each shell. The velocity dispersion was used to assign velocities to individual particles by throwing three random gaussian numbers for each velocity vector. The velocity distribution was isotropic. This procedure generates a system with the NFW profile which is almost in equilibrium. The shot noise (the finite number of particles) results in residual deviations from the equilibrium. The finite extent of the system also produces transient effects at the outer boundary. By running an isolated system with 3000 particles for a long time (five billion years) we tested that the system is really close to a stationary NFW halo. We found only one deviation. The density distribution at the outer boundary (within 30% of  $R_{200}$ ) was slightly smeared out.

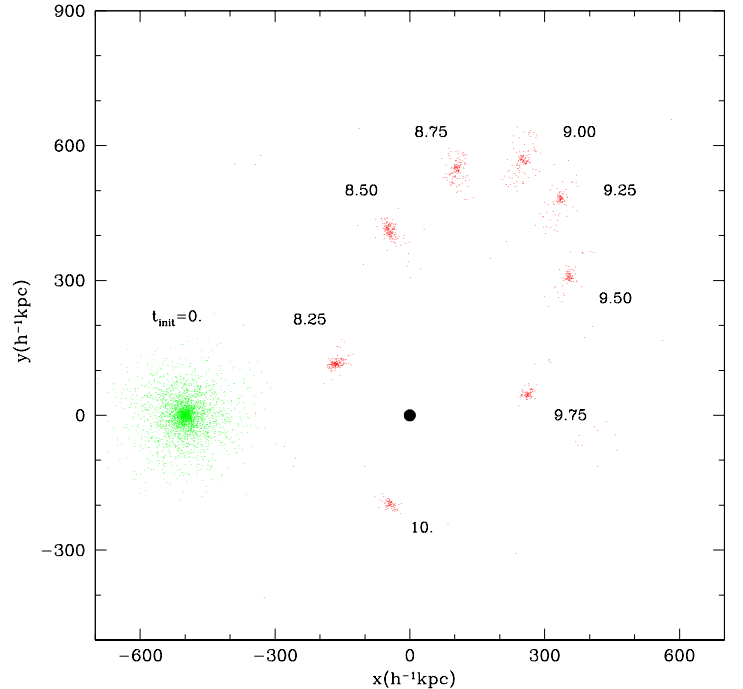


FIG. 4.— Positions of bound particles for halo presented in Figure 3. The time (marked next to the halo) is given in billions of years. The solid circle indicates position of the cluster center. The halo initially had 952 particles and has lost most of its mass after 10 Gyrs. Nevertheless, even after 10Gyr, it can still be identified as a compact centrally concentrated bound lump of particles.

With the exception of the shot noise, no deviations were found inside 70% of  $R_{200}$ .

We use the Aarseth's N-body presented in Binney & Tremaine (1987). The code was modified to include the acceleration from the cluster. The code uses Plummer softening of the gravitational potential. The softening is thus parameterized by a softening length  $\epsilon$ . It should be noted that the Plummer model gives a softer force as compared with the ART code, which we used for large-scale simulations. We estimate that the difference in resolution is about factor of two: 10% error in acceleration is reached at  $\sim 2$  cells in ART code as compared with  $\sim 3.7\epsilon$  in a code with the Plummer softening (Kravtsov et al. 1997).

As a typical example, we have chosen an elliptical orbit with the minimum distance to the cluster center of  $200h^{-1}\text{kpc}$  and ratio of maximum to minimum distances of 3.35. Initially the halo was placed at distance  $500h^{-1}\text{kpc}$  and was given velocity  $710\text{ km s}^{-1}$  (circular velocity at that distance) in the direction of 45 degrees to the radius. The period of the resulting orbit is  $2 \times 10^9\text{ yrs}$ . The tidal radius at pericenter was  $37h^{-1}\text{kpc} \approx 1.9R_s$  and mass within the tidal radius was 1/3 of the halo's initial virial mass. We study the effects of the force and mass resolution on the evolution of the halo varying the resolutions by a factor of 20.

Figure 3 shows the evolution of the total bound mass (top panel) and the bound mass inside central  $20h^{-1}\text{kpc}$  (middle and bottom panels). We show the results only if more than 15 bound particles are

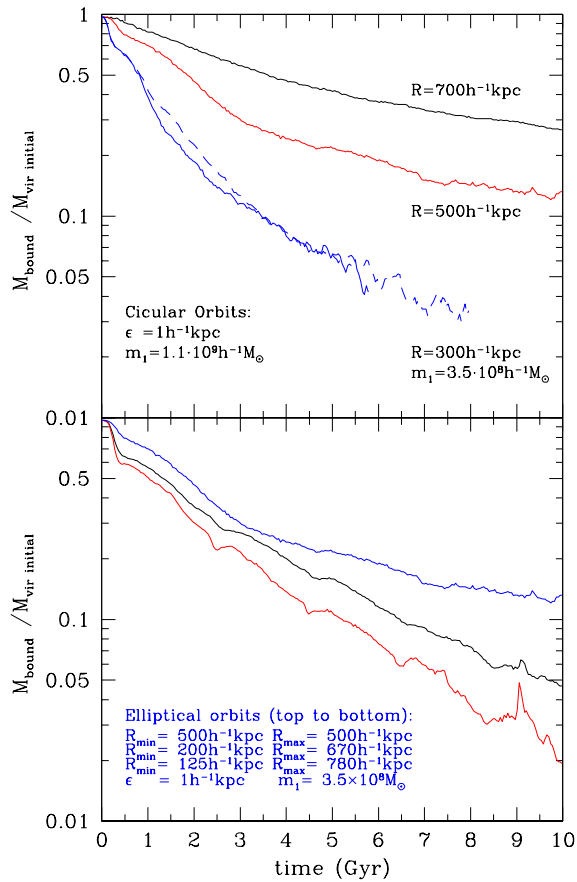


FIG. 5.— Mass evolution for halos on different orbits. While halos on the highly eccentric orbits, with pericenters as small as  $125h^{-1}\text{kpc}$ , have survived for at least 10Gyr, a halo on a circular orbit with radius  $300h^{-1}\text{kpc}$  was tidally destroyed after about 7 Gyrs regardless of the used resolution. Note that improving mass resolution by a factor of three allows us to track the halo for a longer time. But results indicate convergence at mass fractions above 5%.

found in the central region. The halo is considered “lost” if the number of bound particles is less than 15. For halos in the middle panel we fixed the mass resolution and studied the effect of the force resolution. If the force resolution is not sufficient, the halo is lost. For example, with the force resolution of  $\epsilon = 10h^{-1}\text{kpc} \approx R_s/2$  the halo is lost after 4Gyr. Increasing the force resolution helps the halo to survive, but once a threshold of  $\epsilon = (1 - 2)h^{-1}\text{kpc}$  is reached, additional increase in resolution does not change the mass of bound particles, which indicates convergence of the results. Extra resolution may even reduce the bound mass because of excessive two-body scattering, which was observed in some of our simulations.

The bottom panel of Figure 3 illustrates the effects of the mass resolution. In this case the force resolution was fixed to  $\epsilon = 1h^{-1}\text{kpc}$ , sufficient for halo survival with mass resolution  $m_1 = 1.05 \times 10^9 h^{-1} M_\odot$  of the previous plot. The halo with three times worse mass resolution was lost after 6.5Gyr. As in the case of varying force resolution, the increase of mass resolution above some limit does not result in increase of the bound mass, which again points to convergence. This can be seen more clearly in the top panel: when the mass resolution is improved by a factor of 6 (from the dotted to the solid curve), the mass of bound

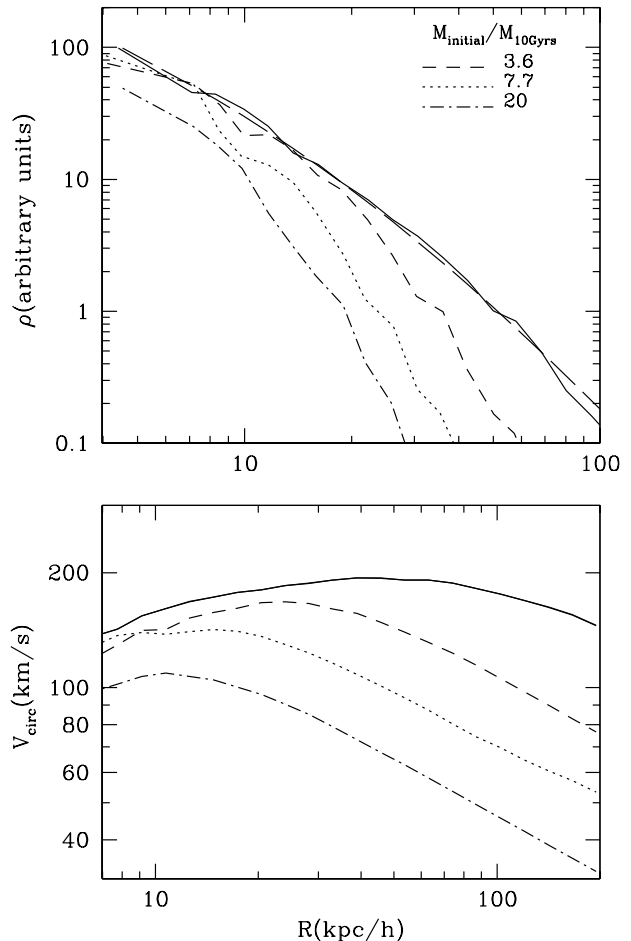


FIG. 6.— The evolution of density (top) and velocity (bottom) profiles for a halo of mass  $10^{12}h^{-1} M_\odot$  orbiting inside a  $2 \times 10^{14}h^{-1} M_\odot$  cluster. In both panels, the *solid* curves show initial profile; the *long dashed* curve in the top panel shows the NFW profile for the initial distribution; *short-dashed*, *dotted*, and *dot-dashed* curves show profiles for halos on different orbits after 10 Gyrs of orbiting in the cluster. The orbits of the halos are the same as the two top curves in panels of Figure 5 (one orbit is shown twice). The curves correspond to different initial to final mass ratios (shown in the legend). Note that the central  $\sim 10$  kpc region is less affected by the tidal stripping, but when the halo loses more than 90% of its mass even the center becomes affected noticeably.

particles changes only by 10%-15%.

It should be stressed that the mass loss of the halo was really dramatic: after 10Gyr the halo was 20 times less massive than at the beginning. The mass of the whole halo is a function of time, which steeply declines in the beginning and tends to level out at later moments. The mass loss from the central region behaves as a step function: after every passage near the cluster center the mass drops by 20% – 30%. Nevertheless, the halo has survived (i.e., was detectable) for at least 10Gyr. Figure 4 illustrates the dramatic mass loss of the halo. In this plot we show only bound particles for a halo which initially had 952 particles. While the halo has lost most of its mass, even after 10 Gyr it is still a compact centrally concentrated dense lump of particles.

Survival or destruction of halos depends on parameters



of their orbits in the cluster. To study the orbit dependence, we have run similar simulations varying orbit eccentricities and radii. We have found that in general halos on circular orbits suffer larger mass loss than halos on the eccentric orbits. Although the pericenter of the latter may be smaller, the halos spend only a small fraction of the orbital period in the central dense region of cluster. Figure 5 shows mass evolution for halos on different orbits. While halos on the highly eccentric orbits, with pericenters as small as  $125h^{-1}\text{kpc}$ , have survived for at least 10 Gyr, a halo on a circular orbit with a radius of  $300h^{-1}\text{kpc}$  was tidally destroyed after  $\approx 7$  Gyrs, regardless of the used resolution.

Finally, Figure 6 shows evolution of the density and circular velocity ( $V_c(r) = \sqrt{GM(< r)/r}$ ) profiles of the halo for the same orbits as shown in Figure 5 during a 10 Gyr period of orbital evolution. Different orbits lead to different mass loss rates and the figure shows the cases in which the ratio of initial to final bound halo mass is 3.5, 7.7, and 20. The figure shows that significant mass loss results in dramatic changes of the density and velocity profiles at large radii. The changes, however, are not as dramatic for the central halo regions. Nevertheless, in the case of extreme mass loss ( $\approx 95\%$ ) shown by the dot-dashed curves, both density and maximum circular velocity decrease by a factor of two from their initial values.

### 2.5. Erasure of substructure via dynamical friction

The dynamical friction is another effect that contributes to the erasure of the substructure. This is not a numerical effect, but by driving galaxies to the cluster center where they will be tidally destroyed, it can enhance numerical effects. The dynamical friction time for a small halo with mass  $m$  moving on a circular orbit of radius  $R$  around the large halo can be estimated using the Chandrasekhar's formula (Binney& Tremaine 1987) with assumptions of equilibrium and a Maxwellian isotropic distribution of velocities of the DM particles. The rate of the orbital radius decay due to the dynamical friction is given by

$$\begin{aligned} \frac{dR}{dt} &= -\frac{2R}{t_{fric}} \left( \frac{\partial \ln M(R)}{\partial \ln R} + 1 \right), \\ t_{fric} &= \frac{V_{circ}^3}{4\pi G^2 (\ln \Lambda) m(r_t) \rho(R) [\text{erf}(X) - 2Xe^{-X^2}/\sqrt{\pi}]}, \\ V_{circ}^2 &= GM(R)/R, \quad X = \frac{V_{circ}}{\sqrt{2}\sigma_r} \\ \ln \Lambda &= \ln \left( \frac{R_{vir}}{R} \frac{M(R)}{m(r_t)} \right), \\ M(R) &= -\frac{R\sigma_r^2}{G} \left[ \frac{d \ln \rho}{d \ln R} + \frac{d \ln \sigma_r^2}{d \ln R} \right]. \end{aligned} \quad (8)$$

For the density profile Eq.(1) we have  $d \ln \rho / d \ln R = -(1+3x)/(1+x)$ , where  $x = R/R_s$ . The last of the equations (8) can be rewritten as an equation for the velocity dispersion:

$$\frac{d\sigma_r^2}{dx} - \frac{1+3x}{x(1+x)}\sigma_r^2 = -\frac{GM_{vir}}{R_s f(C)} \cdot \frac{f(x)}{x^2} \quad (9)$$

The solution of the equation is

$$\sigma_r^2 = \frac{x(1+x)^2}{4} \left[ \sigma_0^2 - 4 \frac{GM_{vir}}{R_s f(C)} \int_1^x \frac{f(x)}{x^3(1+x)^2} dx \right]$$

$$\begin{aligned} &= V_{max}^2 \frac{2x(1+x)^2}{f(2)} \int_x^\infty \frac{f(x)}{x^3(1+x)^2} dx \\ \sigma_0^2 &= 4 \frac{GM_{vir}}{R_s f(C)} \int_1^\infty \frac{f(x)}{x^3(1+x)^2} dx \approx 0.432 V_{max}^2. \end{aligned} \quad (10)$$

Here  $\sigma_0$  is the 1D velocity dispersion at  $R = R_s$ . The velocity dispersion  $\sigma_r$  has a maximum  $\sigma_r \approx \sigma_0$  at  $R \approx 0.8R_s$ . It declines on smaller and larger radii, but the maximum is flat:  $\sigma_r \approx 0.78\sigma_0$  at  $R = 0.1R_s$  and  $\sigma_r \approx 0.69\sigma_0$  at  $R = r_{vir}$ . Equations (8) and (10) define the dynamical friction time, which is presented in Figure 7 for different masses of clusters and halos. For a given halo, the dynamical friction time decreases as the halo moves into the cluster because the density of cluster increases. Note, however, that this decrease is countered by the halo mass decrease due to the tidal stripping. The dynamical friction time is thus a varying quantity which depends on the cluster mass, distance from the cluster center, and halo's gravitationally bound mass.

We should note that equation 8 should be considered as a rough estimate of the effect for at least two reasons. First, we assume for simplicity that orbits are circular, which, of course, is a very simplified view of the real halo orbits in clusters. This simplification, however, makes it possible to estimate all the interesting quantities analytically and thus greatly facilitates computations of dynamical evolution. There is very little data as to what kinds of orbits are to be expected (see, however, recent work of van den Bosch et al. 1998). Recent numerical studies by Tormen (1997), Tormen et al (1998), and Ghigna et al. (1998) give somewhat different accounts on the distribution of the orbital parameters. Tormen (1997) concludes that orbits are neither radial nor circular and that the average eccentricity of the orbits is  $\epsilon \approx 0.5$ , while orbits in cluster analyzed by Ghigna et al. (1998) are reported to be mostly radial. It is not clear at present what causes the difference.

Importance of the dynamical friction for a particular halo will depend on the halo's orbit. Halos on circular or low-eccentricity orbits with large radius will experience little gravitational drag and would never come close to the center and get tidally disrupted. On an eccentric orbit, some of these objects would have a chance to pass through the dense cluster core where the tidal effects discussed in the previous section (and gravitational drag too) would be considerably stronger. Note, however, that the time spent by a halo on highly eccentric orbit near the orbit pericenter is rather small. The strong tidal force in the cluster center will shock the halo during pericenter passages, but for most of its orbit the halo will exist in less dense (and thus more favorable for its survival) environments. The worst evolution scenario can be envisioned for a halo on a low-eccentricity orbit with a small radius. Such halo will suffer both strong and continuous tidal losses and fast decay of the orbital radius due to the dynamical friction.

The validity of the Chandrasekhar's formula in spherically symmetric, finite-size systems was also a subject of extensive debate over the years. One obvious drawback of this equation is that it does not predict a drag experienced by a satellite on an orbit outside of the spherical

system (e.g., Lin & Tremaine 1983). Most studies, however, indicate that the equation works remarkably well. Lin & Tremaine (1983), for example, have addressed the subject numerically and have found that eq. 8 works well for satellites of mass  $\lesssim 0.05$  of the primary. The same conclusion was reached in other numerical studies (Bontekoe & van Albada 1987; Zaritsky & White 1988; or more recently, Cora et al. 1997). Analytical study by Weinberg (1986), in which Chandrasekhar’s formula was rederived for spherically symmetric potential, also shows that this formalism is applicable in most cases. Recent analytical studies by Bekenstein & Maoz (1992), Maoz (1993), and Domínguez-Tenreiro & Gómez-Flechoso (1998) used fluctuation-dissipation approach to derive the energy losses due to the gravitational drag. Despite the more sophisticated treatment and inclusion of the various important details (satellite’s size, not negligible mass of the background particles, inner velocity structure of satellite), it appears that Chandrasekhar’s formula gives a good approximation for the energy losses.

Domínguez-Tenreiro & Gómez-Flechoso (1998), for example, have taken into account both the finite size of the satellite and the internal velocity structure of the satellite. Their analysis shows that if internal velocity dispersion of the satellite is  $\lesssim 0.5$  of the velocity dispersion of the primary system (always the case in our study of massive clusters) the energy losses predicted by Chandrasekhar’s formula are accurate to within  $\sim 30\%$ .

There is, of course, a considerably larger uncertainty caused by the choice of the Coulomb logarithm, because there is no general prescription of how to estimate the minimum and maximum impact parameters. The value of the Coulomb logarithm in clusters of galaxies is expected to be  $\ln \Lambda \approx 5 - 10$ . The value of  $\ln \Lambda = 8$  was used in a recent study by Tormen et al. (1998), who compared dynamics of dark matter halos in clusters in the cosmological context. They showed that even when  $\ln \Lambda$  is kept constant the Chandrasekhar’s formula works remarkably well, predicting quite accurately decay of the satellite’s orbital radius for the satellites as massive as  $\sim 0.2 - 0.5$  of the cluster mass. This latter test is most relevant to our study and shows that use of the eq. 8 is justified.

The dynamical friction time as a function of the distance to the cluster center for a variety of cluster and satellite masses is shown in figure 7. In general, the results are hardly surprising. Dynamical friction in rich clusters  $M_{\text{vir}} \approx 10^{15} h^{-1} M_{\odot}$  is negligible except for the most massive galaxies near the cluster center. For poor clusters and groups with  $M_{\text{vir}} \lesssim 10^{14} h^{-1} M_{\odot}$ , the friction time is short as compared with the Hubble time. Adding the baryons would only shorten the friction time, as more mass would be retained within the halo’s tidal radius. If a group exists for a sufficiently long time and does not accrete efficiently new satellites, the dynamical friction would produce an object that would look like an overmerger – a giant central galaxy with no other galaxies in the group<sup>4</sup>. The epoch of formation and the growth rate of groups depends on the parameters of a cosmological model. Thus, if resolution is sufficient to make the numerical effects negligible, excessive overmerging for groups and poor clusters should indicate that the cosmological model is wrong.

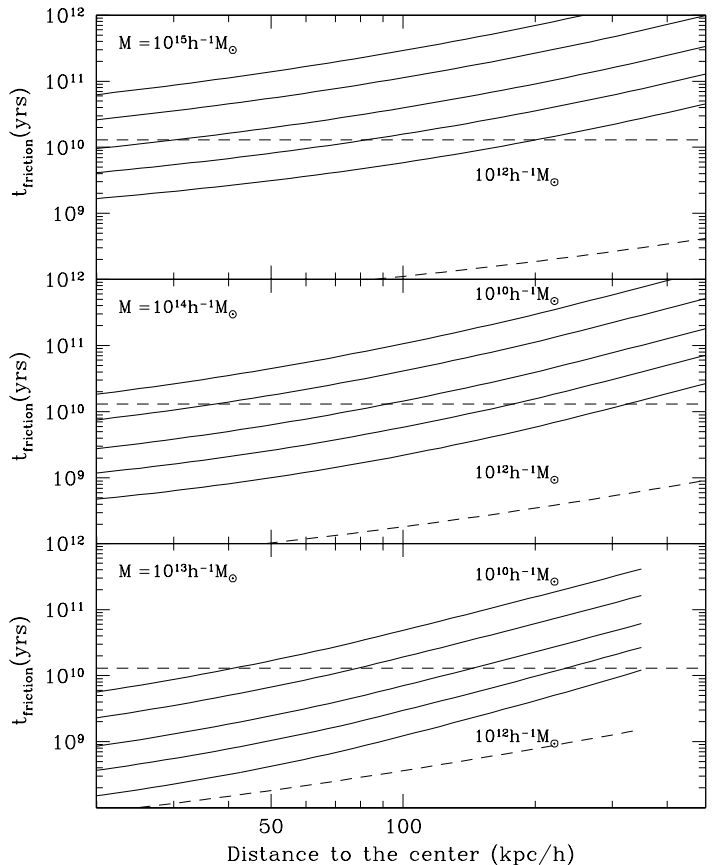


FIG. 7.— The dynamical friction time for different masses of clusters and halos. For a given halo the dynamical friction time decreases as the halo moves into the cluster because the density of cluster increases. But then the halo starts to lose its mass, and the friction time increases again. The set of virial masses is the same as in Figure 1. The horizontal dashed line shows the Hubble time for this cosmological model.

A matter of concern is how one could distinguish between numerical and physical effects as the primary cause of overmerging. There may be two approaches to this problem. First, one can estimate the required resolution in the manner outlined in the next section and run a simulation. After that run another simulation with considerably higher resolution. Such a test may be prohibitive in terms of the CPU time required to run the very high-resolution run. However, it is probably the most certain way of testing for the numerical effects. High-resolution simulations of individual clusters are probably best suited for this kind of test. Indeed, a similar test was attempted by Ghigna et al. (1998), who analyzed two runs of the same clusters with different spatial resolutions. The second possible solution is to identify cluster’s progenitor at an earlier epoch (e.g.,  $z = 1$ ) and follow evolution of a sample of test halos in the representative mass range. This analysis may show what mechanism is really at work (e.g., dynamical friction may be clearly observed in the orbit decay) and may allow one to estimate whether the numerical resolution is adequate.

<sup>4</sup>Notably, such systems are observed in the real Universe (Carignan et al. 1997).

### 2.6. What numerical resolution is required?

Numerical experiments presented by Moore et al. (1996) show that halos become unstable and get quickly disrupted if tidal radius is smaller than  $\sim 2-3$  times the core radius. The force softening,  $r_{soft}$ , usually has effect of creating an artificial core in the density distribution at scales  $\lesssim r_{soft}$ . Thus, it can be assumed (optimistically) that halos get disrupted if  $r_t \lesssim 2r_{soft}$ . The details of the tidal stripping will, of course, depend non-trivially on the mass and orbital parameters of halo. However, tidal radius for a halo can be approximately defined (Johnston 1998; Ghigna et al. 1998) as the tidal radius defined by equations 6,7 at the pericenter of the halo orbit. Numerical studies of satellite dynamics (e.g., Johnston, Hernquist & Bolte 1996) indicate also that  $\sim 10-30\%$  mass loss can be expected at every pericentric passage, which agrees well with results of our numerical experiments. This will have an additional effect if halo orbits long enough to make several pericentric passages.

Thus, with an adequate mass resolution, dark matter halos should survive (at least during the first period of their orbit) inside groups of galaxies as long as their pericentric  $r_t$  is twice or larger than the force resolution. These halos may lose a large fraction of their mass, but they should be able to retain their identity even without the additional baryonic dissipation. If the required force resolution cannot be achieved, the baryons need to be included to alleviate the problem.

Ultimately, survival of a particular halo will depend on both the mass and the force resolution. In order for two-body evaporation to be negligible, halos must contain  $\gtrsim 30$  particles. This will define the mass limit for the surviving halos even if the force resolution is sufficiently high. A very optimistic estimate, thus, would be that a halo should consist of at least  $\sim 20-30$  particles and its tidal radius should be larger than two resolution elements.

As an example, we consider a rather typical simulation with particle mass of  $10^{10}h^{-1} M_\odot$  and the resolution of  $30h^{-1}\text{kpc}$  (e.g., Gelb & Bertschinger 1994; Ma & Bertschinger 1995; Tormen 1997). With this resolution one would naively hope to find  $\approx 10^{11}h^{-1} M_\odot$  satellites – the virial radius of a halo with this mass is more than twice larger than the force resolution. The top panel in Figure 1(b) indicates, however, that halos of this initial virial mass cannot be found inside a cluster of mass  $10^{14}h^{-1} M_\odot$ : due to the insufficient mass resolution they lose so much of their mass that they are destroyed by the tidal force. The mass resolution of these simulations was sufficient to find what is left of a halo with  $3 \times 10^{11}h^{-1} M_\odot$  at distances  $\gtrsim 80h^{-1}\text{kpc}$ . However, the bottom panel in Fig. 1(b) shows that tidal radius for galaxy-size halos is smaller than two resolution elements within central  $\sim 300h^{-1}\text{kpc}$  and thus no such halos should be expected there. Therefore, lack of the force resolution resulted in erasure (“overmerging”) of even fairly massive ( $\sim 10^{12}h^{-1} M_\odot$ ) halos within the  $300h^{-1}\text{kpc}$ .

But even a considerably better resolution may not be sufficient if we deal with a really massive cluster. For example, Carlberg (1994) simulated a  $2.2 \times 10^{15}h^{-1} M_\odot$  cluster with mass resolution of  $2.27 \times 10^9h^{-1} M_\odot$  and the Plummer force softening of  $\epsilon = 9.7h^{-1}\text{kpc}$ . According to Gelb & Bertschinger (1994), the effective resolution

for the Plummer force is  $2.6\epsilon$ . This gives the resolution  $\approx 25h^{-1}\text{kpc}$ , which we use as a limit on the tidal radius of resolved halos. Analysis of tidal radii for a cluster of this mass shows that due to the insufficient force resolution, no halos should exist at distances smaller than  $\lesssim 290h^{-1}\text{kpc}$ . Halos of mass  $M_{vir} < 10^{11}h^{-1} M_\odot$  should be tidally destroyed at  $R = 590h^{-1}\text{kpc}$ . This is consistent with what Carlberg (1994) found in his simulation.

What resolution is required for halos to survive? The above examples show that the answer depends on the mass of the cluster and on the mass of the halo one would like to resolve. The force resolution should be (significantly) smaller than the minimal tidal radius of a halo (defined by the orbit’s pericenter). For a  $10^{14}h^{-1} M_\odot$  cluster the tidal radius for a massive halo of mass  $M_h \gtrsim 10^{11}h^{-1} M_\odot$  at a distance of  $R \gtrsim (60-70)h^{-1}\text{kpc}$  is  $r_t \approx 10h^{-1}\text{kpc}$ . The force resolution should probably be better than  $3h^{-1}\text{kpc}$  for such halo to survive in the cluster. Because the halo at this distance loses 80%–90% of its original virial mass, and because realistically one needs at least 20–30 particles to identify a halo, the particle mass should be smaller than  $\approx 10^9h^{-1} M_\odot$ . These estimates may be optimistic for halos that orbit in cluster for several periods due to continuing mass loss (see §2.2) and possible effects of halo-halo heating (Moore et al. 1996).

To some extent, the answer is clear. In order to allow a galaxy-size halo to survive, the force resolution must be much smaller than its tidal radius and the halo must be represented by many particles. For a typical large galaxy of the mass  $10^{11}h^{-1} M_\odot$  and tidal radius of  $10h^{-1}\text{kpc}$  in a  $\sim 10^{14} - 10^{15}h^{-1} M_\odot$  cluster, the resolution must be of  $(0.5-3)h^{-1}\text{kpc}$  and particle mass  $\lesssim 10^9h^{-1} M_\odot$ . There is a number of further caveats related to analysis of the halo remnants. The most important of them is the question of whether it is possible to recover properties of the original halo from the properties of the remnant. Unfortunately, the answer to this question is not clear and various parameters may be affected in different and complicated ways. Most of the the halos orbit in cluster for periods less than 10 Gyrs, and although their peripheral parts are being stripped, the evolution of the central regions is not dramatic (see Fig. 6).

### 3. SIMULATIONS

We simulate the evolution of  $128^3$  cold dark matter particles in two cosmological models: a flat low-matter density CDM model with cosmological constant ( $\Lambda\text{CDM}$ ;  $\Omega_0 = 1 - \Omega_\Lambda = 0.3$ ;  $h = 0.7$ ;  $\sigma_8 = 1.0$ ) and a model with a mixture of cold and hot dark matter (CHDM;  $\Omega_0 = 1$ ;  $\Omega_\nu = 0.2$ ;  $h = 0.5$ ;  $\sigma_8 = 0.7$ ). The CHDM simulation followed trajectories of additional  $2 \times 128^3$  hot particles. The mass fraction of hot matter,  $\Omega_\nu$ , is equally split between two types of neutrino (Primack et al. 1995). Both models were normalized to be consistent with *COBE* DMR observations (Bunn & White 1997). Normalization of the  $\Lambda\text{CDM}$  model is also consistent with observed abundance of galaxy clusters (Viana & Liddle 1996), while normalization of the CHDM model may be slightly higher than suggested by the data (Gross 1997). Both simulations are initialized with the same set of initial random numbers in order to reduce effects of the cosmic variance.

To achieve sufficiently high mass resolution, the size of

the simulation box for both the  $\Lambda$ CDM and the CHDM models is chosen to be rather small –  $15h^{-1}$ Mpc. To test the effects of the box size, an additional simulation of  $30h^{-1}$ Mpc box has been run for the  $\Lambda$ CDM model. The mass of a cold particle in the  $15h^{-1}$ Mpc box simulations (for  $30h^{-1}$ Mpc box particle mass is 8 times larger) is  $m_1 = 1.33 \times 10^8 h^{-1} M_\odot$  for the  $\Lambda$ CDM model and is  $\approx 2.7$  times larger for the CHDM model. If we assume that  $\gtrsim 30$  particles are needed to identify a halo, we expect to be able to identify halos as small as  $4 \times 10^9 h^{-1} M_\odot$ . This corresponds to  $4 \times 10^{10} h^{-1} M_\odot$  halo before tidal stripping, if 90% of mass was stripped by the cluster.

The simulations were done using the Adaptive Refinement Tree (ART) code (Kravtsov et al. 1997). The code used a  $256^3$  uniform grid on the lowest level of resolution and seven levels of refinement for the  $15h^{-1}$ Mpc box. Each refinement level doubles the resolution. The seventh refinement level corresponds to the dynamical range of 32,000 and the resolution of  $\approx 0.5h^{-1}$ kpc. The  $30h^{-1}$ Mpc run had six levels of refinement and its resolution is  $\approx 2h^{-1}$ kpc. The code refines an individual cell on a given level  $L$  if the number of particles in this cell (as estimated by the cloud-in-cell method) exceeds some threshold  $N_{th}(L)$ . The threshold is  $N_{th} = 5$  for high levels and  $N_{th} = 10$  is set for low levels  $L = 0, 1$  (Kravtsov et al. 1997). This choice of thresholds ensures that refinements are introduced only in the regions of high-particle density and prevents the two-body relaxation effects. The increase in spatial resolution corresponding to each successive refinement level is accompanied by decrease of the integration time-step by a factor of 2. The simulations were started at  $z_i = 30$  when the rms of the density fluctuations in the simulation box was  $\delta \approx 0.27 - 0.32$ .

The dynamic range of the simulation is justified by the following two considerations. First, the code integrates the evolution in *comoving* coordinates. Therefore, to prevent degradation of force resolution in *physical* coordinates, the dynamic range between the start and the end ( $z = 0$ ) of the simulation should increase by  $(1 + z_i)$ : i.e., for our simulations  $256 \times (1 + z_i) = 7680$ . Second, the code reaches its peak resolution in the highest density regions inside virial radius of the DM halos. To resolve a halo, we need at least  $\sim 10$  resolution elements per halo size, which justifies the dynamic range of  $\gtrsim 10,000$ .

Particle trajectories were integrated with the step in expansion factor of  $\Delta a_0 = 0.0015$  on the zero level uniform grid, and with time step  $\Delta a_L = \Delta a_0 / 2^L$  on a refinement level  $L$ . This gives an effective number of steps of 82,000 on the seventh level of refinement. In physical units, the smallest time step at  $z = 0$  corresponds to  $1.15 \times 10^5$  years.

#### 4. HALO IDENTIFICATION

Finding halos in dense environments is a challenge. The most widely used halo-finding algorithms: the friends-of-friends (hereafter FOF, e.g., Davis et al. 1985) and the spherical overdensity algorithm (e.g., Lacey & Cole 1994; Klypin 1996) – are not acceptable (Gelb & Bertschinger 1994; Summers et al. 1995). The friends-of-friends (FOF) algorithm merges together apparently distinct halos if linking radius is too large or misses some of halos if the radius is too small. Adaptive FOF (van Kampen 1995) seems to work better. However, our experiments show that in prac-

tice it is difficult to find an optimal scaling of the linking radius with the density for a general case.

We have developed a version of the FOF algorithm, which we call “hierarchical friends-of-friends”. This algorithm uses a fixed set of hierarchical linking radii and thus does not have problems adaptive FOF algorithm has. The algorithms, either adaptive or hierarchical, cannot work using only geometrical means to identify a halo. In the very dense environments they pick up many fake halos. This can be improved by taking into account dynamical information to decide whether a halo is real or not. The DENMAX algorithm (Bertschinger & Gelb 1991; Gelb & Bertschinger 1994) or its offspring SKID (Governato et al. 1997) make a significant progress – they remove unbound particles, which is important for halos in groups and clusters. Another approach to deal with “flukes” is to check whether the halos in question were distinct halos at earlier epochs.

Recently, Summers et al. (1995) tried to perfect the idea of Couchman & Carlberg (1992) to trace the history of halo merging and to use it for halo identification. Starting at an early epoch, Summers et al. identify halos using the FOF algorithm with linking radius corresponding to the “virial overdensity” of 200 and then trace particles belonging to halos at later times. It appears that it is impossible to make a working algorithm. Halos interact too violently. A large fraction of mass is tidally stripped from some halos and a large fraction of mass is being accreted by others. However, the idea of using a set of epochs is too good to be abandoned. To avoid the problems with the “direct approach” (from past to the future), we have decided to try a reverse logic. Instead of asking the question “where is now the halo that collapsed at some earlier epoch”, we ask “did the halo that we find at present exist at an earlier time?”. Thus, we supplement our hierarchical FOF algorithm with an algorithm which checks if halos existed at previous moments.

The algorithm which finds halos as maxima of mass inside spheres of a given overdensity works better than the plain FOF, but no fixed overdensity limit can find halos in both low and high density environment. However, the attractive simplicity of this algorithm makes it worth in looking for ways of improving it. We will discuss our improvements to such an algorithm in §4.2. Besides the problem of finding whether a halo is real, a problem of “missing” halos should be kept in mind. As was discussed in the previous section, while some halos may survive in dense environments, others may be destroyed due to numerical effects. These halos will be missing at  $z = 0$  and “present to past” approach does not help.

Some of the problems that any halo finding algorithm faces are not numerical. They exist in the real Universe. We select a few of the most typical difficult situations.

1. *A large galaxy with a small satellite.* Examples: the LMC and the Milky Way or the M51 system. Assuming that the satellite is bound, do we have to include the mass of the satellite in the mass of the large galaxy? If we do, then we count mass of the satellite twice: once when we find the satellite and then when we find the large galaxy. This does not seem reasonable. If we do not include the satellite, then the mass of the large galaxy is underestimated. For example, the binding energy of a particle at the distance of the satellite will be wrong. The problem

arises when we try to assign particles to different halos in the effort to find masses of halos. This is very difficult to do for particles moving between halos. Even if a particle at some moment has negative energy relative to one of the halos, it is not guaranteed that it belongs to the halo. The gravitational potential changes with time, and the particle may end up falling onto another halo. This is not just a precaution. This actually was found very often in real halos when we compared contents of halos at different redshifts. Interacting halos exchange mass and lose mass. We try to avoid the situation: instead of assigning mass to halos, we find the maximum circular velocity,  $\sqrt{GM/R}|_{max}$ , which is a more meaningful quantity than mass from observational point of view.

2. *A satellite of a large galaxy.* The previous situation is now viewed from a different angle. How can we estimate the mass or the rotational velocity of the satellite? The formal virial radius of the satellite is large: it coincides with the virial radius of the host halo. In order to find the outer radius of the satellite, we analyze the density profile. At small distances from the center of the satellite the density steeply declines but then it flattens out and may even increase. This means that we reached the outer boundary of the satellite. We use the radius at which the density starts to flatten out as the first approximation for the radius of the halo. This approximation can be improved by removing unbound particles and checking the steepness of the density profile in the outer part.

3. *Tidal stripping.* This is not a numerical effect and is not due to a “lack of physics”. Very likely this is what happens to real galaxies in clusters. Their peripheral parts, responsible for extended flat rotation curves outside of clusters, are lost when the galaxies fall into a cluster. Thus, if an algorithm finds that 90% of mass of a halo identified at early epoch is lost, it does not mean that the halo was destroyed. This is a normal situation. What is left, given that it still has a large enough mass and radius, is a galaxy halo.

#### 4.1. Hierarchical friends-of-friends algorithm

In order to find substructures at vastly different overdensities, we use hierarchical friends-of-friends algorithm (HFOF). This algorithm simply applies the FOF algorithm with a set of different (hierarchical) linking lengths. In our analysis we use 4 hierarchical levels, in which case the set consists of linking lengths starting from the small value  $l_{vir}/8$  and larger values obtained by doubling this value:  $l = l_{vir}/4$ ,  $l = l_{vir}/2$ , and  $l = l_{vir}$ . We call  $l = l_{vir}$  the lowest (with respect to the corresponding overdensity threshold) level and  $l = l_{vir}/8$  the highest level. The linking length  $l_{vir}$  corresponds to the virial overdensity of an object. We assume the virial overdensity of 200 and 340 ( $l_{vir} = 0.2\bar{l}$  and  $l_{vir} = 0.17\bar{l}$ ) for SCDM/CHDM and for  $\Lambda$ CDM models, respectively (e.g., Lahav et al. 1991; Eke et al. 1996); here,  $\bar{l} = n_0^{-1/3}$  is the mean interparticle separation and  $n_0$  is the mean particle density in the simulation box. For our halos the smallest linking length,  $l = l_{vir}/8$ , corresponds to overdensity of  $\approx 10^5$ . At each level of the hierarchy identified clusters of particles (halo candidates) are marked if none of their particles belongs to a marked higher-level cluster. Finding halo candidates first at the highest possible level is important because some of higher-

level clusters merge into larger halos at lower levels. In practice, we find that in high-resolution simulations there is a wealth of small clumps on all levels in large cluster-size halos, defined on the lowest level of the hierarchy  $l_{vir}$ .

Another important feature of this algorithm is use of a particle distribution at an earlier epoch. The FOF algorithm works on a snapshot of the particle distribution and generally tends to identify particle clusters that are linked at this moment just by chance. Typical examples would be either a “bridge” connecting two particle clusters or small satellite clusters on highly eccentric orbit that move temporarily beyond the virial radius of a massive halo. Therefore, one must check the stability of every identified halo candidate. The easiest way to make such a check is to find whether a given halo candidate exists at an earlier moment. We perform such check by running the HFOF algorithm with the same set of linking lengths using positions of particles at  $z = 1$  and check both the existence and one-to-one correspondence of the progenitor particle clusters. We consider a candidate halo to be “stable” if it has one (or two) progenitor(s) and it is the only descendant of the progenitor(s).

Details of this analysis are as follows. We select the two most massive progenitors of each halo and check whether they combined contain more than a threshold number of particles of the halo at  $z = 0$ . We search for these progenitors on the next lower level of hierarchy to take into account the fact that the size of an unevolving object at  $z = 1$  doubles in comoving coordinates. The level is not reduced if it reaches the virial overdensity. We sum the two most massive progenitors in order to allow one major merging. In fact, there are very few cases in which the masses of three progenitors were of the same order of magnitude. We used the thresholds 70%, 50% and 30% of mass of the halo at  $z = 0$ . The threshold 70% is too high: in many cases halos accrete more than 30% of their mass between  $z = 1$  and  $z = 0$ . The algorithm would fail to find many halos with this threshold. On the other hand, there is little difference in the number of identified halos using thresholds of 30% and 50%. However, the algorithm would not find the most massive and the most dense halos in the center of the large groups because the mass of those halos increases substantially between  $z = 1$  and  $z = 0$  due to merging with small halos and accretion of single particles. To avoid this, we also include halos which contain more than a minimum number (100–500) of particles at  $z = 1$ . We found that the result almost does not depend on the chosen number because at  $z = 1$  these progenitors contain already considerably more particles.

The code checks also whether the particles found in the progenitor represent a substantial fraction of its mass. The importance of this criterion is clear from the following example. Close to the very massive and very dense halos the FOF algorithm finds many small clumps. At an earlier moment, all of these small clumps belong to the same progenitor of the massive cluster around which they were found at  $z = 0$ . Each lump, however, represents only a tiny fraction of the progenitor. To avoid misidentifications the algorithm accepts only halos whose particles represent a substantial fraction of the mass of that progenitor. We used values of 10% and 30% as thresholds for the mass fraction of the progenitor. Results are not sensitive to the particular choice of the threshold. Both criteria (total

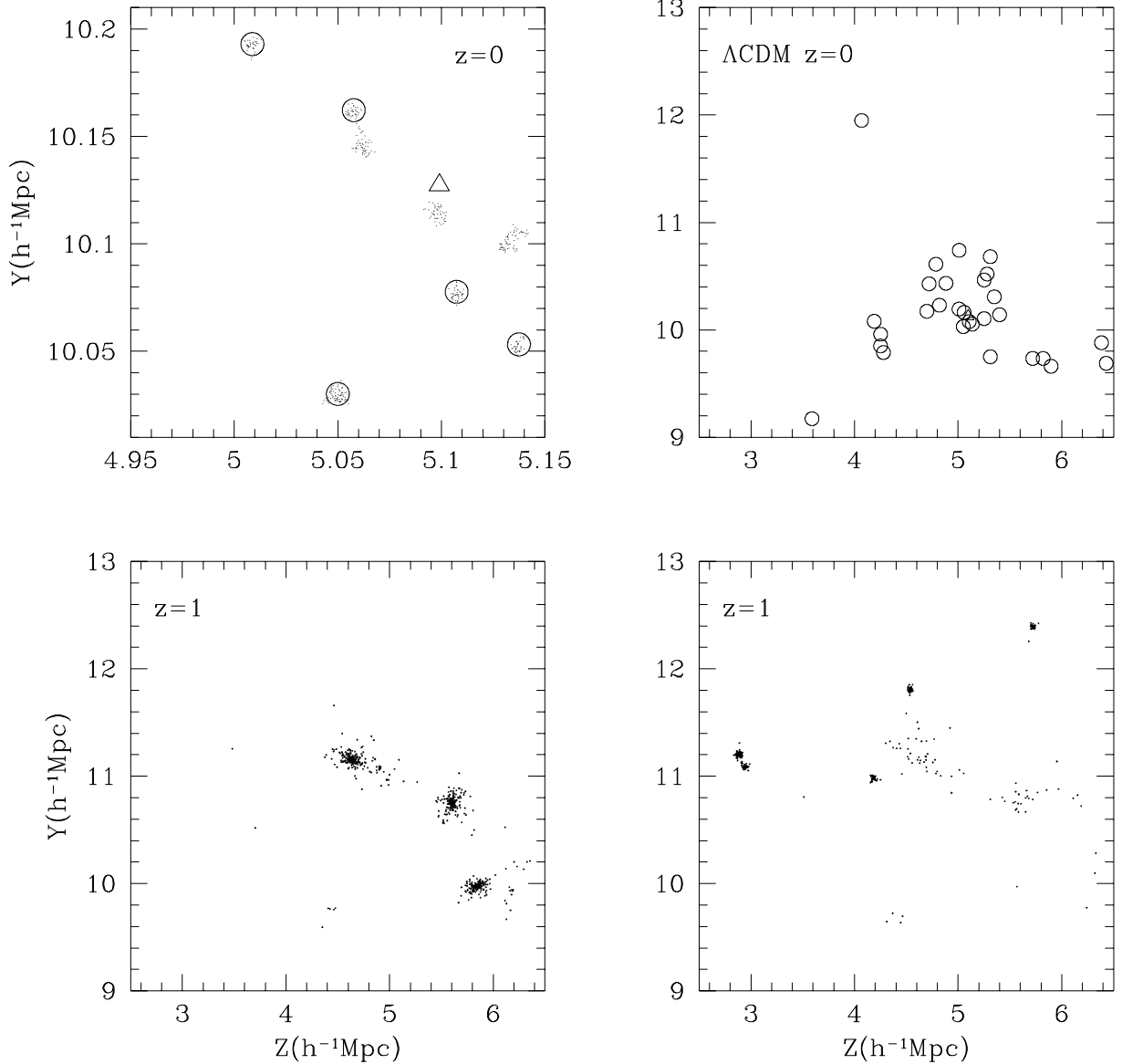


FIG. 8.— A halo identification by the HFOF. *Top row*: Circles and the triangle represent positions of identified halos at the level  $l_{vir}/8$  (overdensity of  $\approx 10^5$ ). Points without circles show fake halos (flukes). Depths of the projections are  $200h^{-1}\text{kpc}$  for the left panel and  $5h^{-1}\text{Mpc}$  for the right panel. *Bottom row*: left panel shows position of dark matter particles of the fake halos at  $z = 1$ , while the “real halos” are shown in the bottom right panel. Most of particles of the five “real halos” are in very compact halos whereas the fake halos are very puffy (spread over large groups seen on the top panel of

mass and mass fraction of the progenitor) result in selection of stable halos.

An example of the halo identification in very dense environment is presented in Figure 8. In the top left panel it shows the inner region of a group-size halo with the triangle denoting the position of the identified extended massive central “galaxy” of the group. The points surrounded by circles represent dark matter particles in five identified halos at the level  $l_{vir}/8$  (overdensity  $\approx 10^5$ ). Points without circles show fake halos (flukes): the halos are found by the FOF algorithm at this level, but they do not satisfy the fraction of progenitor criterion. Bottom left panel shows position of dark matter particles of the fake halos at  $z = 1$ , while the “real halos” are shown in the bottom right panel. Most of particles of the five “real halos” are in very compact halos, whereas the particles of the fake halos are in

extended and “puffy” configurations.

#### 4.2. Bound density maxima algorithm

In addition to the hierarchical FOF, we have developed another halo-finding algorithm, which uses ideas of the DENMAX algorithm (Bertschinger & Gelb 1991; Gelb & Bertschinger 1994). Just as the DENMAX, our algorithm first finds positions of the density maxima on some scale and then removes unbound particles inside the halo radius (hence, the name: Bound Density Maxima (BDM)). However, the algorithm finds maxima and removes unbound particles in a different from the DENMAX way. The algorithm can work by itself or in conjunction with the hierarchical FOF. In the latter case, it takes positions of halos from the HFOF, and then removes unbound particles and finds parameters of halos. The version of the

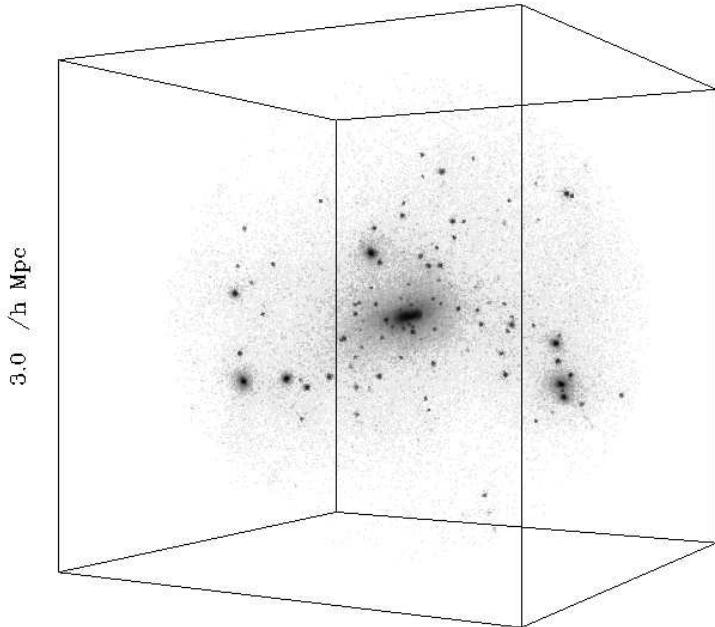


FIG. 9.— An example of a poor cluster in a  $\Lambda$ CDM simulation. At  $z = 0$  the cluster has a virial mass of  $2 \times 10^{13} h^{-1} M_{\odot}$ , virial radius of  $500 h^{-1} kpc$ , and velocity dispersion of  $\sim 500 km/s$ . The figure shows all DM particles ( $\sim 250,000$ ) in a sphere of radius  $1.5 h^{-1} Mpc$  with the centered at the cluster. The particles are color-coded on a grey-scale according to the  $\log_2$  of the local density (the density is estimated as a number of particles at  $r < 8 h^{-1} kpc$  from a given particle). Figure 10 shows the halos identified in this volume by the bound density maxima algorithm.

BDM code used here is available for use by astrophysical community (see Klypin & Holtzman 1997).

In order to find positions of halos we choose a smoothing radius  $r_{sp}$  of a sphere for which we find maxima of mass. This defines the scale of objects we are looking for, but not exact radii or masses of halos. Radius of a halo can be either larger or smaller than  $r_{sp}$ . For example, if we are interested in galaxy-size halos, it is reasonable to choose  $r_{sp} \sim (10 - 15) kpc$ . If we search for galaxy groups, an appropriate choice is  $r_{sp} \sim (200 - 300) kpc$ . Then we place a large number of the spheres in the simulation box. The number of the spheres is typically an order of magnitude or more larger than the number of expected halos. For each sphere we find its center of mass and the mass inside  $r_{sp}$ . The center of the sphere is displaced to the new center of mass and this process is iterated until convergence. Depending on specific parameters of the simulations, the number of iterations ranges from 10 to 100. This process finds local maxima of mass within  $r_{sp}$ . Some of the maxima will be found many times. We remove duplicates and keep only one halo for each maximum. Halos with too

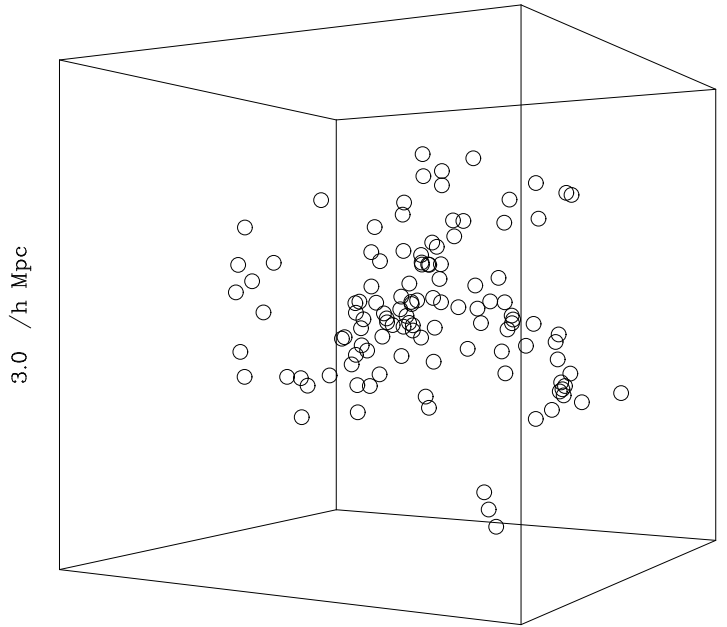


FIG. 10.— Dark matter halos identified by the bound density maxima algorithm in the volume shown in Figure 9 (volume and projection are the same).

small number of particles (typically 5–10) and halos with too low central overdensity are removed from the final list.

Figures 9 and 10 illustrate typical output of the algorithm. Figure 9 shows a group-size halo identified in our  $30 h^{-1} Mpc$   $\Lambda$ CDM simulation. The particles, shown in the figure inside the sphere of radius  $1.5 h^{-1} Mpc$  centered on the group, are color-coded on a grey-scale according to the logarithm of the local density, estimated as a number of particles within  $8 h^{-1} kpc$  of the particle. Figure 10 shows dark matter halos identified by the BDM algorithm in this volume. All of the halos, that can be seen in Figure 9 as tight dark clumps of particles, are identified by the halo finder.

Once centers of potential halos are found, we start the procedure of removing unbound particles and finding the structure of halos. We place concentric spherical shells around each center. For each shell we find mass of the dark matter particles, mean velocity, and the velocity dispersion relative to the mean. In order to determine whether a particle is bound or not, we estimate the escape velocity (Eqs.5) at the position of the particle. If velocity of a

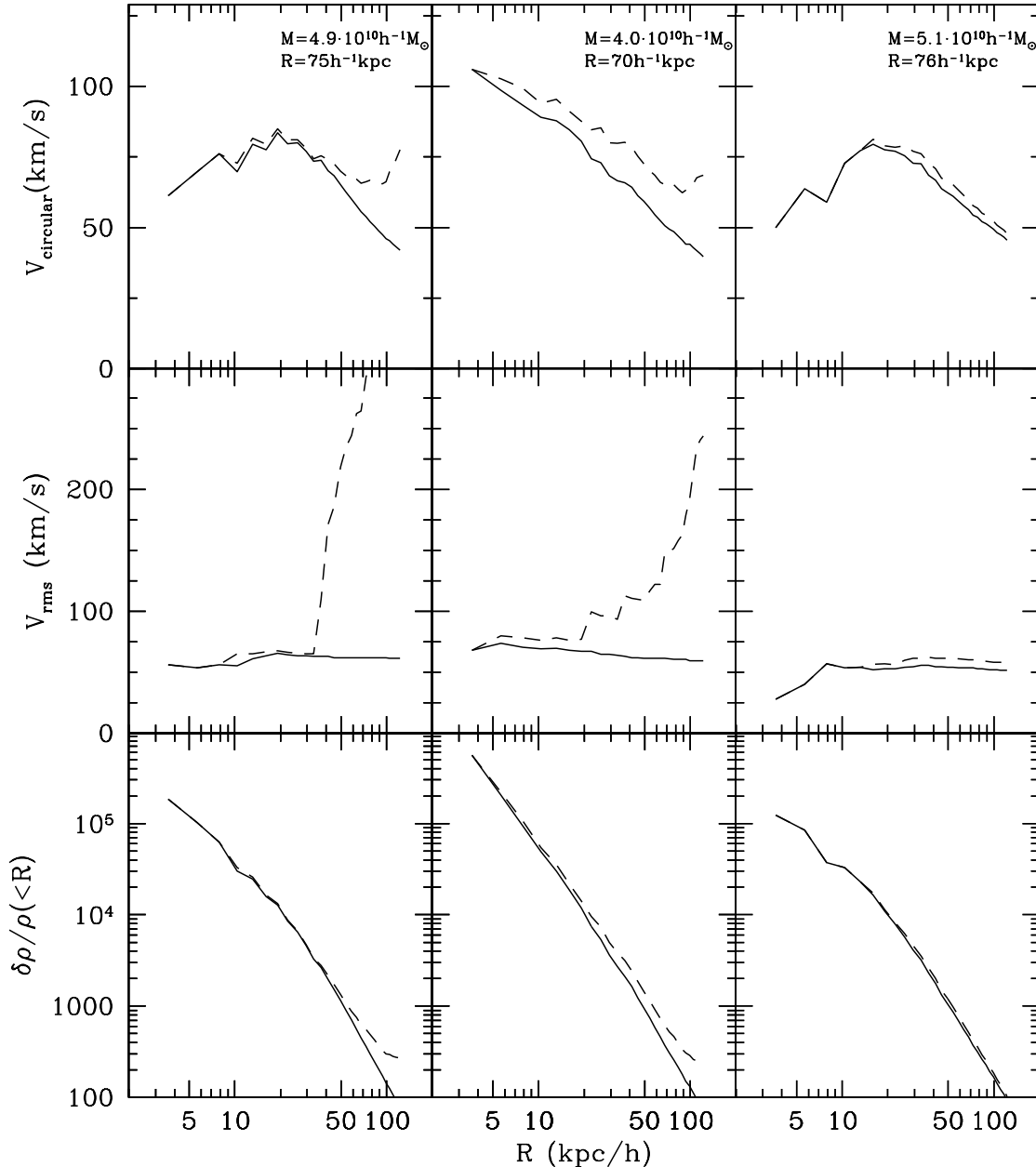


FIG. 11.— Examples of profiles of small halos in the  $\Lambda$ CDM model. Each column of plots corresponds to the same halo. Mass and radius of each halo (within virial overdensity 340) are shown in the top panels. The dashed curves are for the halos before the removal of unbound particles, and the full curves are for bound particles only. The top row of panels shows the circular velocity  $V_{\text{circular}} = (GM(R)/R)^{1/2}$ . The middle row shows velocity dispersion of the dark matter particles, and the bottom row presents the overdensity profiles. The right halo is an example of an isolated halo in which most particles are bound to the halo. The two halos on the left show examples of small satellite close to a large halo. In the central  $\sim 20h^{-1}\text{kpc}$  part of both halos the velocity dispersions are small and almost constant. But at  $30h^{-1}\text{kpc}$  the velocity dispersion starts a dramatic increase indicating presence of a massive object.

particles is larger than the escape velocity, it is assumed to be unbound. We estimate the maximum rotational velocity  $V_{\text{max}}$  and radius of the maximum  $r_{\text{max}} = 2r_s$  using the density profile for the halo. Because  $V_{\text{max}}$  and  $r_{\text{max}}$  must be found before the unbound particles are removed and because the mean velocity is also found using all particles (bound and unbound), the whole procedure can not be done in one step. We start by artificially increasing the value of the escape velocity by a factor of three. Only particles above the limit are removed. We find new density profile, new mean velocities, new  $V_{\text{max}}$  and  $r_{\text{max}}$ . The es-

cape velocity is again increased, but this time by a smaller factor. The procedure is repeated 6 times. The last iteration does not have any extra factors for the escape velocity.

Removal of unbound particles is crucial in the case when a halo with a small internal velocity dispersion moves inside a large group. For example, if a halo with a circular velocity of  $100\text{ km s}^{-1}$  moves with velocity  $500\text{ km s}^{-1}$  inside a group, a dark matter particle bound to the group has kinetic energy 25 times larger than the kinetic energy of a particle of the halo. Even if only 1/10th of particles within the halo radius belong to the group, the whole halo will



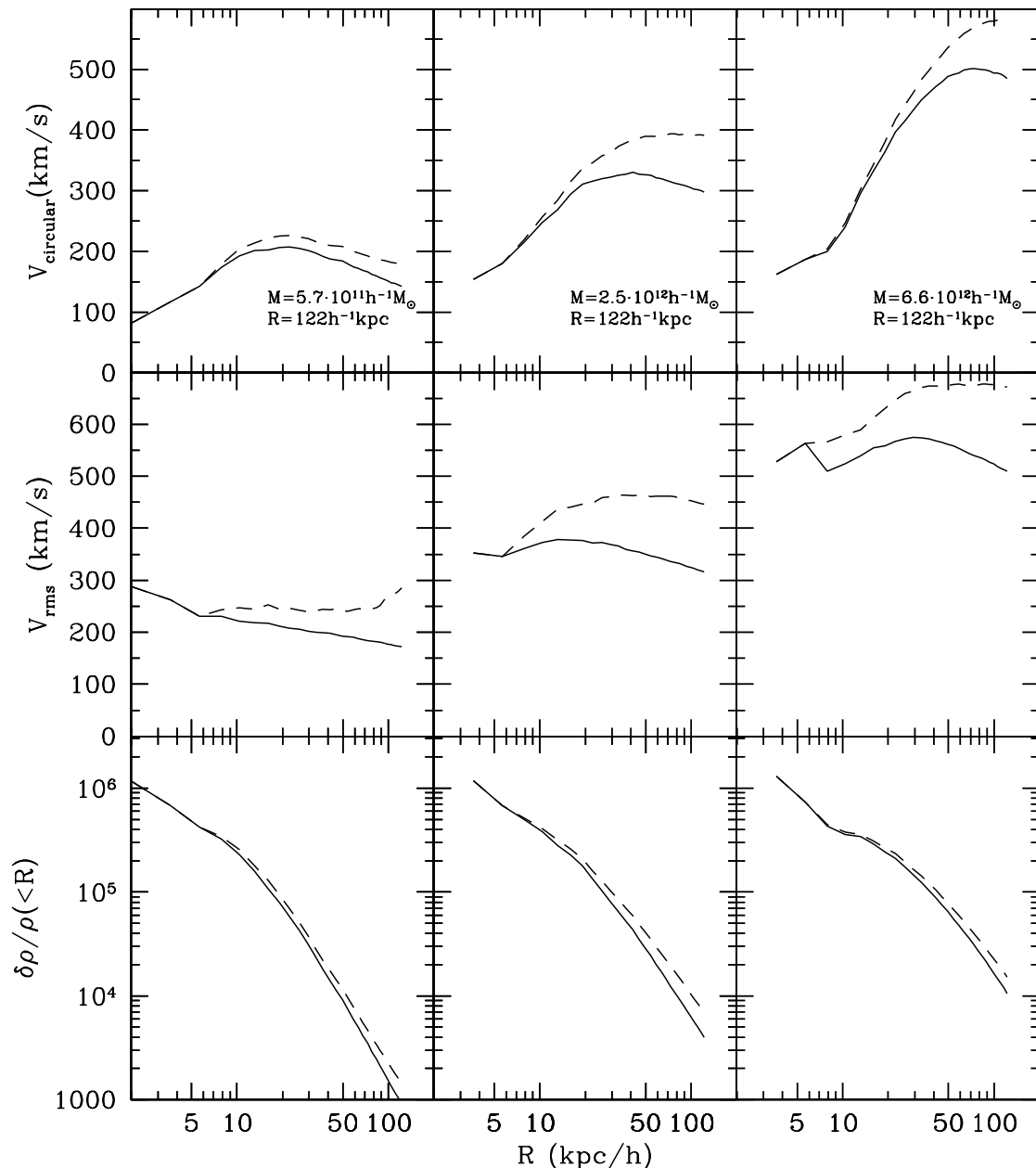


FIG. 12.— The same as in Figure 11 but for medium and large halos. In this case the masses are given for constant outer radius of  $122h^{-1}\text{kpc}$ . The mean overdensity at that radius for all halos is significantly larger than the virial value. But the maximum of rotational velocity is well within the distance.

have positive energy and will be treated as fake. Removal of unbound particles salvages the halo even if the real halo particles constitute as little as 1/4 of the total number of particles within the halo radius. This estimate is valid in the case of a compact halo moving through homogeneous field of high velocity particles of the group. The situation is worse if the particles of the high velocity field are very lumpy. The worst case is the collision of two equal mass halos. At the moment when the halos overlap, the code does not find any bound component – both halos are missed. The chance of such event is very small because the distance between centers of halos should be smaller than  $\sim (10 - 15)h^{-1}\text{kpc}$ .

The effect of the unbound particle removal on the halo

profiles is illustrated in Figures 11 and 12. The halos were identified in the simulation of the  $30h^{-1}\text{Mpc}$   $\Lambda\text{CDM}$  simulation. In the Figure 11 the right column shows circular velocity, velocity dispersion, and density profiles of a “normal” halo with a small fraction of unbound particles, primarily in the outer regions. The middle and left columns show profiles of small satellite halos located inside or close to a massive halo. In the central  $\sim 20h^{-1}\text{kpc}$  of both halos the velocity dispersions are small and almost constant. The circular velocities are about what one should expect for these values of the velocity dispersions. But at  $30h^{-1}\text{kpc}$  the velocity dispersion increases dramatically, indicating a presence of a dense background of fast moving particles belonging to the massive halo. Figure 12 shows

typical examples of medium- and high-mass halos.

#### 4.3. Comparison of the HFOF and BDM algorithms

The goal of both of the described algorithms is to find positions of stable halos in a given simulation. Nevertheless, the two algorithms are quite different. The HFOF, for example, computes mass, spin parameter, angular momentum, shape and total binding energy of the halos without removal of unbound particles. The algorithm, however, does not assume spherical symmetry in these calculations. The BDM algorithm computes properties of the halos (e.g., mass, velocity, density profile) after removing unbound particles, the procedure based on the assumption of spherical symmetry. Therefore, one must expect that the algorithms may compute slightly different properties for the same halos.

Nevertheless, the most important information determined by halo finders is positions of DM halos. Our tests show that the algorithms find exactly the same halos, if the halos contain more than a couple hundred particles. The agreement is about 95 % for halos with more than 50 particles and about 90 % for halos with more than 30 particles. The small differences in the threshold criteria for the selecting halos account for the 10 % differences at the low mass end of the halo distribution. But overall, the agreement is very good. For example, the five small and the big central halo in a high density region shown on the top left panel of Figure 8 have been found by both algorithms. We also compare halos in a statistical way. In Figure 17 we compare the correlation functions of halos found by the two algorithms. For this comparison we have selected halos with rather low limit in maximum circular velocity  $V_{max} > 90$  km/s. In case of the  $\Lambda$ CDM simulation (lower panel) the two correlation functions coincide within the expected scatter due to the statistical noise. This indicates that the thresholds are chosen in an equivalent manner. In case of the CHDM simulation (upper panel) the correlation functions differ more. Very likely this happened because of the slight mismatch in the mass limits. As expected, the two correlation functions differ mainly on scales less than 100 kpc due to different thresholds used in the algorithms.

## 5. RESULTS

### 5.1. Luminosity function of galaxies and $M/L$ in groups

The observed tight correlation between the 21-cm line width  $W \approx 2V_{circ}$  and infrared luminosities for spiral galaxies (e.g., Aaronson & Mould 1983; Bureau, Mould, & Staveley-Smith 1996; Willick et al. 1996; Giovanelli et al. 1997) can be used to estimate luminosities of galaxy-size halos in  $N$ -body simulations (an alternative method for assigning luminosities to the DM halos and constructing the luminosity function was proposed recently by Roukema et al. 1997). This is probably the best one can do when dealing with dissipationless simulations. Unfortunately, the observed Tully-Fisher relation is not defined as accurately as one would hope for. This is especially true for low-luminosity galaxies. In the following, we apply the empirical Tully-Fisher relation determined for galaxies with absolute blue magnitudes  $m_B \leq -15$ .

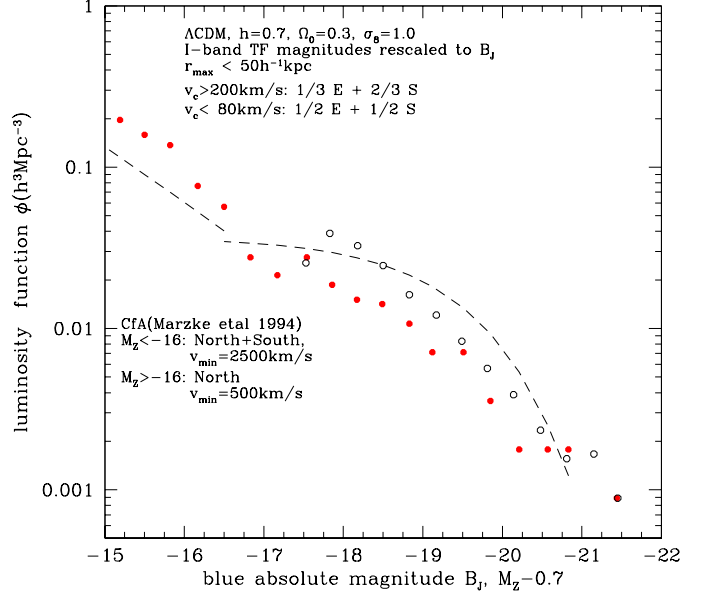


FIG. 13.— Comparison of the luminosity function of galaxy-size halos in the LCDM simulations with the CfA data (dashed curve). The solid circles show results for the  $15h^{-1}$ Mpc box. The results for  $30h^{-1}$ Mpc box are shown with open circles. The first bin of the  $30h^{-1}$ Mpc simulation at  $M = -21.45$  has 8 galaxies; the bin at  $M = -17.8$  has 350 galaxies. There are 146 galaxies brighter than  $B_J = -20$  and 1340 brighter than  $B_J = -18$  in the  $30h^{-1}$ Mpc box simulation.

It should be kept in mind, however, that there may be significant systematic deviations from the relation used here for galaxies with magnitudes of  $m_B > -17$ .

Elliptical galaxies pose another problem. The Faber-Jackson relation indicates that velocity dispersion (and thus the dark matter mass) can be used to estimate galaxy luminosity. The relation, however, is not very tight. In principle, by tracing the merging history of each halo, we can make more realistic estimates of the star formation rates and the luminosities. Here, we will use a simple but reasonable prescription; we assume that an elliptical galaxy is  $\sim 1$  magnitude dimmer than a spiral galaxy with the same maximum circular velocity. This assumption is motivated by the fact that mass-to-light ratio of elliptical is 2.5-3 times higher ratio than that of spirals spirals. It is likely that the fraction of ellipticals is significant only at the high and low mass ends of mass function. We assume therefore that all halos with  $V_{circ} > 350$  km  $s^{-1}$  and half of the halos with  $V_{circ} < 80$  km  $s^{-1}$  host elliptical galaxies. Halos in the “grey area”  $V_{circ} = (200 - 350)$  km  $s^{-1}$  have a gradually increasing probability to host an elliptical:  $\propto 1/3(V/200\text{km/s})^2$ .

It is important to stress the use of maximum circular velocity and/or velocity dispersion of halo as a mass indicator. Problems of finding dark matter halos and determining their masses in numerical simulations highlighted in §4, make it virtually impossible to make a meaningful assignment of mass to a halo in a group or a cluster. On the other hand, velocity dispersion or maximum circular velocity can be determined more or less reliably with even moderate particle statistics.

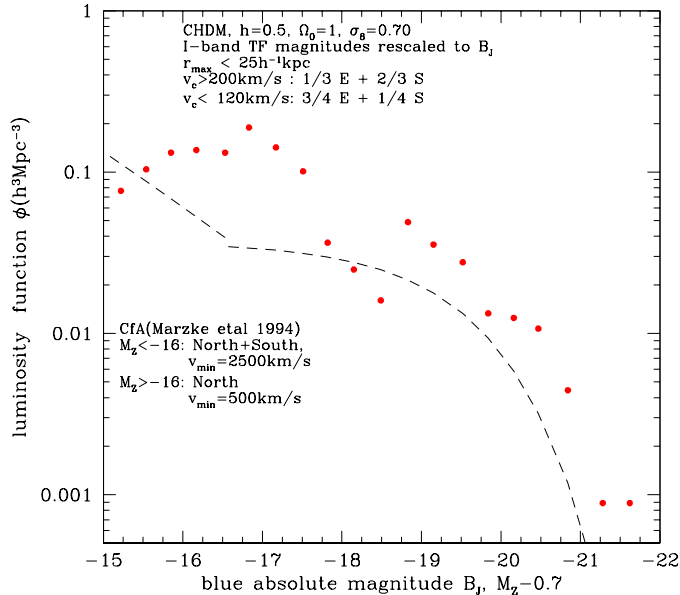


FIG. 14.— The same as in Figure 13, but for the CHDM  $15h^{-1}\text{Mpc}$  box simulation.

We believe therefore that use of the maximum circular velocity as a proxy for halo mass is more attractive than use of potentially unreliable and biased mass estimates.

In order to estimate luminosities of “galaxies” hosted by DM halos using their maximum circular velocities, we use the following Tully-Fisher relation in the I-band:  $M_I - 5\log(h) = -21.0 - 6.8(\log W - 2.5)$ . The slope of the relation is as given from Willick et al. (1996) for field spirals, while the zero point was adopted from Giovanelli et al. (1997). The I-band magnitudes were shifted to the blue magnitudes as  $M_B = M_I + 1.5$  (Pierce & Tully, 1992). Because circular velocities in observations are never measured at large galactocentric distances, we set an upper limit of  $r_{max} < 50h^{-1}\text{kpc}$  for the radius of the maximum of the rotational velocity.

The main caveat of the above luminosity assignment scheme is that we use the maximum circular velocities of halos, discarding the disk contribution. However, as we have discussed in §2.3, this may result in maximum error of 30% in the circular velocity. Also, Figure 6 shows that maximum circular velocity of halos orbiting in clusters may decrease by  $\sim 20-50\%$  due to the tidal stripping. The luminosity assignment may be somewhat biased for such halos if baryons are not stripped as efficiently as the dark matter.

Figure 13 shows the luminosity function (LF) of galaxy-size halos identified in the two of our  $\Lambda\text{CDM}$  simulations. The solid circles show results for the  $15h^{-1}\text{Mpc}$  box. There is a significant tail of low luminosity galaxies ( $B_J > -16.5$ ), which matches the corresponding tail of the CfA luminosity function (Marzke et al. 1994) and the luminosity function of cluster galaxies (Smith et al. 1997; Lopez-Cruz et al. 1997). The simulation of the larger box of  $30h^{-1}\text{Mpc}$  (open circles) has insufficient mass resolution to probe this low-mass tail, but the two LFs are consistent in the region of overlap. We believe that the LFs in Figure 13 are most reliable in the magnitude range of  $B_J = -17 - 20$ . In this range the number of of ha-

los in each luminosity bin is sufficiently high to make the poisson errors insignificant and results do not depend on the assumed fraction of ellipticals or on the maximum allowed radius for the circular velocity. The first bin of the  $30h^{-1}\text{Mpc}$  simulation at  $M = -21.45$  contains 8 halos, while the bin at  $M = -17.8$  contains 350 halos. The luminosity function in the  $\Lambda\text{CDM}$  model in this range of magnitudes is systematically lower by a factor of 1.5–2 than the CfA luminosity function. This is consistent with deeper samples, which give lower normalization for the luminosity function (e.g., Loveday et al. 1992).

The luminosity function of galaxy-size halos in the CHDM simulation is significantly higher than both the  $\Lambda\text{CDM}$  and the CfA luminosity functions. With the same set of parameters as for the  $\Lambda\text{CDM}$  model, the LF in the CHDM model is a factor of 4–5 higher than the luminosity function in the CfA catalog. In order to reconcile the model with the observational data, we reduced the limit on the radius for the rotational velocity to  $r_{max} = 25h^{-1}\text{kpc}$  and raised the fraction and the limiting magnitude for small elliptical galaxies. Figure 14 shows the CHDM luminosity function that best matches the CfA luminosity function. It is still systematically higher than the CfA LF, but it might be acceptable due to small volume of the simulation.

## 5.2. Halo dynamics in groups: velocity bias, $M/L$ , and constraints on $\Omega$

The observed mass-to-light ratios of galaxy groups and clusters,  $(M/L)_B \approx 150 - 400$  (e.g., Bahcall, Lubin & Dorman 1995), are often used as an argument in favor of the low-density universe with  $\Omega_0 \approx 0.2 - 0.3$ . We have used the halos identified in poor galaxy clusters and groups in our simulations to study their dynamical properties and estimate the mass-to-light ratio of these clusters using the same prescription to assign luminosity to halos as was used in the previous section. Figures 15 and 16 present different properties of groups of galaxies in the simulations. Centers of the groups were found using search radius of  $r_{sp} = 0.250h^{-1}\text{Mpc}$  and no removal of unbound particles was done in this case. Radius of groups was estimated at the overdensity limit of 200 for the CHDM model and of 340 for the  $\Lambda\text{CDM}$  model. The results clearly indicate that the  $M/L$  ratio increases with the mass of the group. However, there is an indication that in the  $\Lambda\text{CDM}$  simulation  $M/L$  ratio for massive groups flattens at the level of  $\approx 300h^{-1}(M_\odot/L_\odot)$ . Note, that models with  $\Omega_0 = 0.3$  ( $\Lambda\text{CDM}$ ) and  $\Omega_0 = 1$  (CHDM) reproduce the observed  $M/L$  ratios equally well, although due to the small volume, we can only probe masses of  $\lesssim 3 \times 10^{13}h^{-1} M_\odot$  in the CHDM simulation. It appears thus that mass-to-light ratio of galaxy groups of mass  $\lesssim 3 \times 10^{13}h^{-1}M_\odot$  is not a very good indicator of the total matter density in the universe.

Several authors have suggested a possible existence of the velocity bias  $b_v \equiv \sigma_{halo}/\sigma_{dm}$ : systematic difference between rms velocities of galaxies and dark matter particles (Carlberg, Couchman & Thomas 1990; Carlberg 1994; Colafrancesco, Antonuccio-Delogu & Del Popolo 1995). The existence of the velocity bias would have impact on the determination of cluster masses using galaxy dynamics and other analyses.

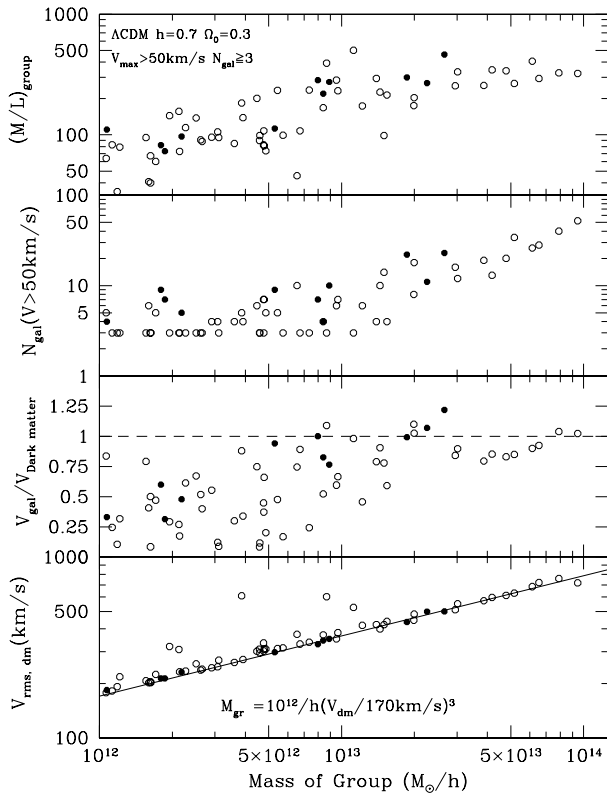


FIG. 15.— Properties of groups in the  $\Lambda$ CDM simulations as a function of the total mass of the group.  $V_{rms,dm}$  is the root-mean-square velocity of dark matter particles in the group. The ratio of the rms velocities of galaxies in the group to  $V_{rms,dm}$  is shown in the second panel. Results for groups with more than 3 satellites are shown. In small groups with mass less than  $10^{13} h^{-1} M_{\odot}$  there is on average a significant velocity bias, which is likely related to the dynamical friction. There is no indication of the velocity bias for larger groups. The number of galaxies with  $V_{circ} > 50 \text{ km s}^{-1}$  in a group is shown in the third panel from the bottom. The mass-to-light ratio of groups (in units of  $h^{-1} M_{\odot} / L_{\odot,B}$ ) is shown in the top panel.

Figures 15 and 16 show that there is no evidence for strong velocity bias for halos in groups in our simulations; on average, for objects  $\gtrsim 10^{13} h^{-1} M_{\odot}$  the rms velocities of galaxies and dark matter particles are equal. Although theoretical arguments suggest that a mild velocity bias should exist (due, for example, to effects of dynamical friction), the uncertainties of current simulations favor absence of the velocity bias ( $b_v = 1$ ) and excludes values of the bias  $b_v \lesssim 0.8$ , allowing, however, for a possible existence of a mild bias  $b_v \approx 0.8 - 0.9$ . Note that for small groups of galaxies ( $10^{12} h^{-1} M_{\odot} \lesssim M_{vir} \lesssim 10^{13} h^{-1} M_{\odot}$ ) a significant velocity bias is observed. This bias could probably be attributed to the strong dynamical friction effects operating in these systems.

### 5.3. Small scale two-point halo correlation function

Analyses of recently completed galaxy surveys resulted in a very accurate determination of the galaxy two-point correlation function,  $\xi(r)$ , at the scales of  $\gtrsim 20 - 50 h^{-1} \text{kpc}$  (e.g., Baugh 1996). The comparison of the observed  $\xi(r)$  with the two-point correlation function of mass in dissipationless  $N$ -body simulations has shown that an antibias of galaxies is required at small scales in order to reconcile the

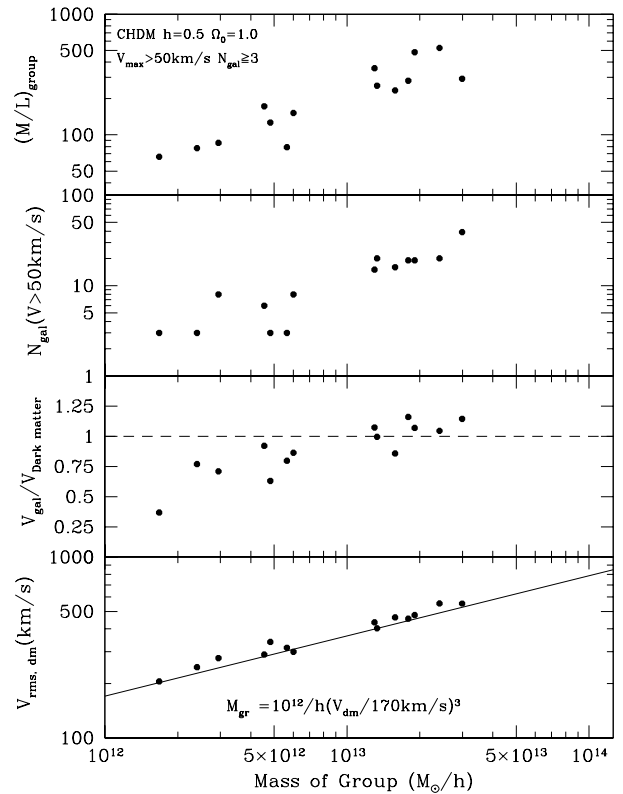


FIG. 16.— Properties of groups in the CHDM simulation.

models with observations (Klypin, Primack & Holtzman 1996; Jenkins et al. 1998). In order to check whether any significant antibias exists for the dark matter halos (which could be associated with observed galaxies), we have constructed the halo-halo two-point correlation function for the halos found in our simulations using both hierarchical friend-of-friend and bound density maxima algorithms. Figures 17 and 18 show correlation functions of halos and dark matter in the simulations. The correlation function is clearly affected at scales  $\gtrsim 500 h^{-1} \text{kpc}$  by the finite box size (as shown by comparison of  $\xi(r)$  for small and large box simulations of the  $\Lambda$ CDM model). However, it is interesting to examine the relative behavior of the dark matter and halo correlation functions at scales  $\lesssim 500 h^{-1} \text{kpc}$ . At very small scales (less than  $100 h^{-1} \text{kpc}$ ) the galaxies are more clustered (biased) relative to the dark matter; at larger scales the effect is the opposite: galaxies are slightly antibiased. This is observed in all simulations and it is valid for all limits on masses of galaxies. It is interesting that the antibias of the magnitude 0.7–0.9 seen in the Figure 17 is almost exactly what is needed for the  $\Lambda$ CDM model to be compatible with observational data on the power spectrum in the range of wavenumbers  $k = (0.1 - 1) h \text{Mpc}^{-1}$  (Klypin et al. 1996; Smith et al. 1998; Jenkins et al. 1998). The antibias of halos at these small scales is very likely related to the tidal destruction and dynamical friction of halos in groups. The  $100 h^{-1} \text{kpc} - 1 h^{-1} \text{Mpc}$  range is the range where we expect both of these processes to work. This conjecture seems to be confirmed by results of larger simulations (Colín et al. 1998; Kravtsov & Klypin 1999).

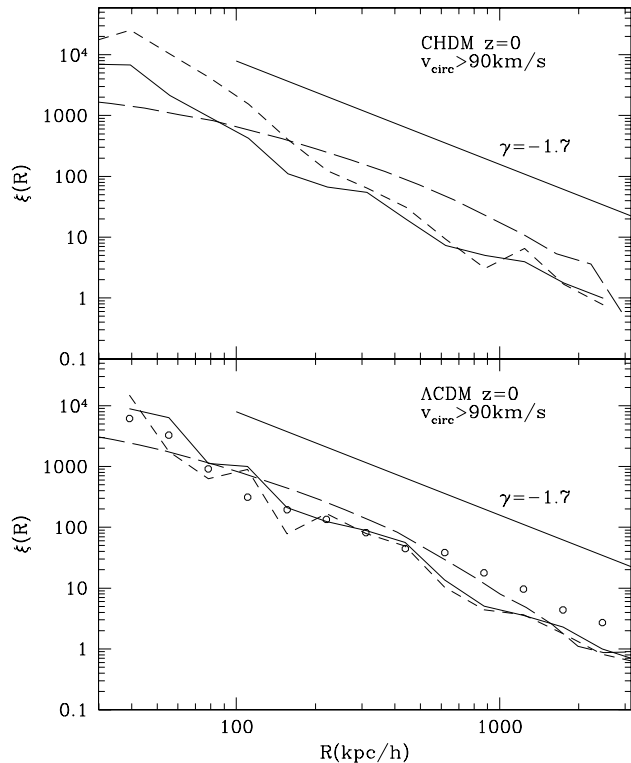


FIG. 17.— Correlation functions of the dark matter (long dashed curves) and galaxy-size halos in the  $\Lambda$ CDM (bottom) and the CHDM simulations (top) in the  $15h^{-1}$ Mpc boxes. Galaxies with rotational velocity larger than  $90 \text{ km s}^{-1}$  were selected. Short-dashed curves are for galaxies identified with the hierarchical friends-of-friends algorithm. The solid curves are for halos identified using bound density maxima algorithm. The circles are for halos identified using the bound density maxima algorithm in the  $30h^{-1}$ Mpc box simulation with the same limit on the rotational velocity.

## 6. CONCLUSIONS

We have presented arguments that the overmerging problem is mostly due to inability of a numerical code to provide a sufficient numerical resolution to prevent tidal destruction of galaxy-size halos by the tidal forces of group or cluster and have estimated the resolution needed to prevent such disruption. We argue that although energy dissipation by the baryonic component helps galaxies to survive in clusters, at distances  $\gtrsim (50 - 70)h^{-1}$ kpc from the cluster center the gravity of the dark matter alone is enough to keep them alive.

The main result of this work is estimate of the numerical resolution needed to overcome the overmerging problem. The results of our analytic estimates and numerical experiments show that although it is feasible to overcome overmerging in pure  $N$ -body simulations, resolution required to avoid artificial destruction of galaxy-size halos (mass  $\gtrsim 10^{11}h^{-1}M_{\odot}$ ) is quite high. For viable CDM models and realistic halo profiles this resolution is  $\lesssim 2h^{-1}$ kpc in force and  $\lesssim 10^9h^{-1}M_{\odot}$  in mass. This requires simulations of  $> 10^7$  particles with dynamic range of  $10^5$  in spatial resolution for statistically significant cosmological volumes ( $\sim 100$ Mpc), which remains challenging with the current computers and numerical codes.

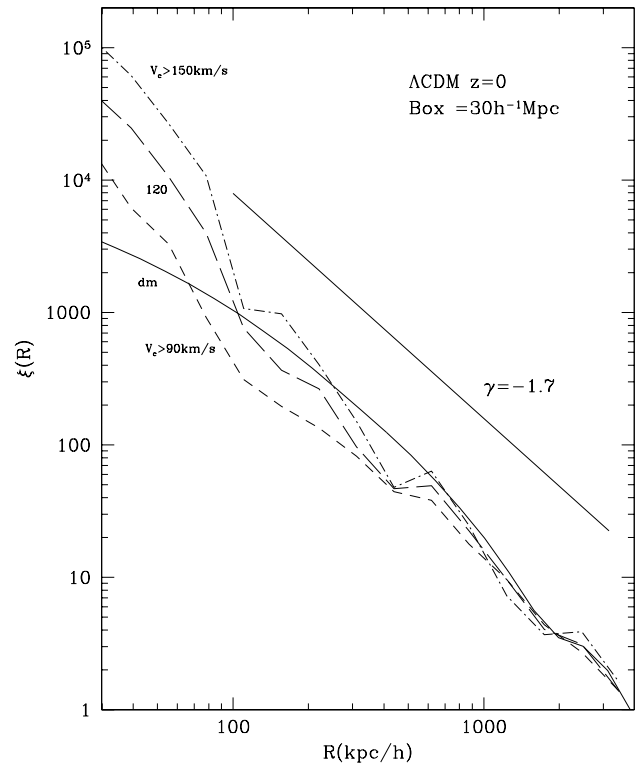


FIG. 18.— Dependence of the galaxy correlation function on mass in the  $\Lambda$ CDM simulation of  $30h^{-1}$ Mpc box. The correlation function increases with the rotational velocity, but all curves show the same tendency: positive bias on small scales, slight antibias on  $(100 - 1000)h^{-1}$ kpc scales, and no bias on larger scales. Absolute values of the correlation functions are affected by the finite box size.

This makes simulations focused on the individual clusters of the type presented in Ghigna et al. (1998) a viable alternative.

Unfortunately, even in the case of sufficient resolution, when halos do survive, the identification of the DM halos in the cores of galaxy groups and clusters in purely dissipationless simulations remains a challenge. In the environments that dense, most of halo's dark matter will be tidally stripped, which makes it difficult to identify the leftover on the very dense, smooth background of high-velocity dark matter particles streaming around and through the halo. We have presented two new halo finding algorithms designed to identify satellite halos located inside the virial radius of a more massive host halo: the hierarchical friends-of-friends and bound density maxima algorithms. Both of our algorithms find practically the same halos, which are stable (existed at previous moments) and gravitationally bound.

To exploit the fact that overmerging is (at least to a certain degree) “beaten” in our simulation, we consider several statistics of galaxy-size halos in our simulations and compare them to the corresponding observed statistics of galaxies. We use a simple scheme, based on the empirical Tully-Fisher relation, to assign a luminosity to the DM halos. The luminosity function of “galaxies” (i.e., galaxy-size halos assigned a luminosity) in the  $\Lambda$ CDM model reproduces the luminosity function of the CfA catalog (Marzke et al. 1994) reasonably well. Both the simulations and the

CfA catalog have an upturn in the number of faint galaxies ( $m_B > -17$ ). However, magnitudes of faint “galaxies” in the simulations rely on a highly uncertain extrapolation of the Tully-Fisher relation and on uncertain assumption about the fraction of elliptical galaxies at these magnitudes. The number of “galaxies” predicted by the CHDM simulation is significantly higher than in the case of the  $\Lambda$ CDM simulation with the same initial random numbers. We failed to produce as nice a fit to the observational data as for the  $\Lambda$ CDM simulation. At this stage it is difficult to judge if this is a significant problem for the model or not. Due to the small size of our simulation boxes, one may argue that simulations with a large box will tend to produce lower luminosity function keeping at the same time the M/L of galaxy groups intact. Larger simulations are needed to clarify the situation.

The mass-to-light ratios of galaxy groups in the simulations  $\sim (200 - 400)h^{-1}$  match those observed reasonably well. It was argued (e.g., Bahcall, Lubin, & Dorman 1995) that dynamics of galaxy groups favors the low- $\Omega$  Universe. Our results show that mass-to-light ratios of groups of mass  $\lesssim 3 \times 10^{13}h^{-1} M_\odot$  is insensitive to the matter density. The halos in the CHDM model are clustered more strongly than the dark matter and one cannot save the argument for a low- $\Omega$  Universe by assuming that groups in the CHDM model have too large fraction of galaxies. It seems that groups occupy too small fraction of the volume and thus their M/L ratios are not representative for the Universe as a whole.

Comparison of the halo and matter correlation functions indicates that halos are antibiased on 100 kpc – 1 Mpc scales. The antibias of the magnitude 0.7–0.9 found in the simulations is needed for the  $\Lambda$ CDM model to be compatible with observational data on the power spectrum in the range of wavenumbers  $k = (0.1 - 1)h\text{Mpc}^{-1}$  (Klypin et al. 1996; Smith et al. 1998). We attribute the antibias to the dynamical friction in groups of galaxies. The friction tends to drag some galaxies to the very central part of groups where they merge the central galaxy and disappear (see

Kravtsov & Klypin 1999 for a more detailed analysis).

Results of this paper can be used in design of the future numerical simulations. We have shown that efficient halo finding algorithms can be developed to identify gravitationally bound satellite halos inside the virial radius of the other halos. Our analytical estimates and numerical experiments show that the numerical resolution required to overcome the overmerging, although quite high, can be achieved with current numerical codes and computer hardware. The main challenge is thus purely computational. This is also true for the simulations that include dissipative hydrodynamics; while alleviating or obliterating some of the problems of dissipationless simulations, they are computationally more intensive. Both numerical approaches have a number of caveats and potential biases, which could only be avoided with inclusion of more realistic physics. The latter appears to be unavoidable, because we cannot reliably predict observed galaxy properties (and hence mimic the selection criteria of the observational catalogs) without realistic physics. Fast increase in computational capability of modern computers and recent developments of new efficient numerical algorithms make the perspective for advances in this direction look good.

We thank Joel Primack for careful reading of the manuscript and comments, Simon White for discussions, and anonymous referee for constructive criticism and useful suggestions which have helped to improve content and presentation of the paper. We are grateful to Avishai Dekel for providing us with computer resources at the Hebrew University. This work was funded by the NSF and NASA grants to NMSU, and the collaborative NATO grant CRG 972148. SG acknowledges support from Deutsche Akademie der Naturforscher Leopoldina with means of the Bundesministerium für Bildung und Forschung grant LPD 1996. Our simulations were done at the National Center for Supercomputing Applications (Urbana-Champaign, Illinois) and on a Power Challenge supercomputer at Hebrew University.

## REFERENCES

- Aaronson, M., & Mould, J. 1983, *ApJ*, 265, 1  
 Avila-Reese, V., Firmani, C., & Hernandez, X., 1998, *ApJ*, accepted  
 Bahcall, N., Lubin, L., Dorman, V. 1995, *ApJ*, 447, L81  
 Baugh, C.M. 1996, *MNRAS* 280, 267  
 Bekenstein, J. D., Maoz, E. 1992, *ApJ*, 390, 79  
 Bertschinger, E., & Gelb, J.M. 1991, *Comp. Phys.*, 5, 164  
 Binney, J., & Tremaine, S. 1987, “Galactic Dynamics” (Princeton: Princeton University Press)  
 Bontekoe, Tj. R., van Albada, T. S. 1987, *MNRAS*, 224, 349  
 Brighenti, F., & Mathews, W.G. 1997, *astro-ph/9707070*  
 Bunn, E.F., & White, M., 1997, *ApJ*, 480, 6  
 Bureau, M., Mould, J.R., & Staveley-Smith, L. 1996, *ApJ*, 463, 60  
 Carignan, C., & Freeman, K. C. 1988, *ApJ*, 332, L33  
 Carignan, C., Côté, S., Freeman, K.C., & Quinn, P.J. 1997, *AJ*, 114, 1313  
 Carlberg, R.G, Couchman, H.M.P., Thomas, P.A. 1990, *ApJ* 352, L29  
 Carlberg, R.G. 1994, *ApJ*, 433, 468  
 Carrol, S.M., Press, W.H., & Turner, E.L. 1992, *ARA&A*, 30, 499  
 Colín, P., Klypin, A.A., Kravtsov, A.V., Khokhlov, A.M. 1998, *ApJ* submitted (preprint [astro-ph/9809202](#))  
 Cora, S. A., Muzzio, J. C., Vergne, M. M. 1997, *MNRAS*, 189, 253  
 Colafrancesco, S., Antonuccio-Delogu, V., Del Popolo, A. 1995, *ApJ* 455, 32  
 Couchman, H.P.M., & Carlberg, R. 1992, *ApJ*, 389, 453  
 Courteau, St., & Rix, H.-W. 1997, *astro-ph/9707290*  
 Davis, M., Efstathiou, G., Frenk, C.S., & White, S.D.M. 1985, *ApJ*, 292, 371  
 de Blok, W.J.G., McGaugh, S.S. 1997, *MNRAS*, 290, 533  
 Dominguez-Tenreiro, R., & Gómez-Flechoso, M.A. 1998, *MNRAS*, in press  
 Eke, V.R., Cole, S., & Frenk, C.S. 1996, *MNRAS*, 282, 263  
 Evrard, A.E. 1997, *MNRAS*, 292, 289  
 Faber, S.M., & Gallagher, J.S. 1979, *ARA&A*, 17, 135  
 Forman, C., Jones, C., & Tucker, W. 1985, *ApJ*, 293, 102  
 Gelb, J., & Bertschinger, E. 1994, *ApJ*, 436, 467  
 Ghigna, S., Moore, B., Governato, B., Lake, G., Quinn, Th., Stadel, J. 1998, *MNRAS*, 300, 146  
 Giovanelli, R., Haynes, M., da Costa, L., Freudling, W., Salzer, J., & Wegner, G. 1997, *ApJ*, 477, L1  
 Governato, F., Moore, B., Cen, R., Stadel, J., Lake, G., & Quinn, Th. 1997, *New Astronomy*, 2, 91  
 Gross, M.A.K., 1997, PhD Thesis, UC Santa Cruz (available electronically at <http://fozzie.gsfc.nasa.gov/index.html>)  
 Jenkins, A. et al., 1998, *ApJ*, 499, 20  
 Johnston K.V., 1998, *ApJ*, 495, 297  
 Johnston, K.V., Hernquist, L., & Bolte, M. 1996, *ApJ*, 465, 278  
 Katz, N., Hernquist, L., Weinberg, D.H., 1992, *ApJ* 399, L109  
 Klypin, A.A., Primack, J., Holtzman, J. 1996, *ApJ*, 466, 13  
 Klypin, A.A. 1996, in “Dark Matter in the Universe”, p. 419, eds. S. Bonometto, J.Primack, A. Provenzale, IOS Press, Amsterdam, Oxford, Tokyo, Washington DC  
 Klypin, A.A., & Holtzman, J. 1997, preprint [astro-ph/9712217](#) (the code is available at <http://astro.nmsu.edu/~aklypin/pmcode.html>)  
 Kravtsov, A.V., & Klypin, A.A. 1999, in preparation

- Kravtsov, A.V., Klypin, A.A., & Khokhlov, A.M. 1997, *Astrophys. J. Suppl.*, 111, 73
- Lacey, C., Cole, S. 1994, *MNRAS*, 271, 676
- Lahav, O., Lilje, P.B., Primack, J.R., & Rees, M.J. 1991, *MNRAS*, 251, 128L
- Lin, D.N.C., & Tremaine, S. 1983, *ApJ*, 264, 364
- Lopez-Cruz, O., Yee, H.K.C., Brown, J.P., Jones, C., & Forman, W. 1997, *ApJ*, 475, 97L
- Loveday, J., Peterson, B.A., Efstathiou, G., Maddox, S.J., 1992, *ApJ*, 390, 338
- Ma, C.-P. & Bertschinger, E. 1995, *ApJ*, 434, L5
- Maoz, E. 1993, *MNRAS*, 263, 75
- Martimbeau, N., Carignan, C., & Roy, J.-R. 1994, *AJ*, 107, 543
- Marzke, R., Geller, M., Huchra, J., & Corwin, H. 1994, *AJ*, 108, 437
- Merritt, D. 1985, *ApJ*, 289, 18
- Mo, H.J., Mao, S., White, S.D.M., 1998, *MNRAS*, 295, 319
- Moore, B., Katz, N., & Lake, G. 1996, *ApJ*, 457, 455
- Navarro, J., Frenk, C., & White, S.D.M. 1995, *MNRAS*, 275, 720
- Navarro, J., Frenk, C., & White, S.D.M. 1996, *ApJ*, 462, 563 (NFW)
- Navarro, J., Frenk, C., & White, S.D.M. 1997, *ApJ*, 490, 493
- Persic, M., Salucci, M., & Stel, F. 1996, *MNRAS*, 281, 27
- Pierce, M., & Tully, B. 1992, *ApJ*, 387, 47
- Primack, J., Holtzman, J., Klypin, A., & Caldwell, D. 1995, *Phys. Rev. Lett.*, 74, 2160
- Rix, H.-W. 1997, *Proceedings of the DM 1996 workshop*, Sesto, astro-ph/9611040
- Roukema, B.F., Peterson, B.A., Quinn, P.J., Rocca-Volmerange, B. 1997, *MNRAS* 292, 835
- Rubin, V.C., Burstein, D., Ford, W.K., & Thonnard, N. 1985, *ApJ*, 289, 81
- Smith, C., Klypin, A., Gross, M., Primack, J., & Holtzman, J. 1998, *MNRAS*, 297, 910
- Smith, R., Driver, S., & Phillipps, S. 1997, *MNRAS*, 287, 415
- Summers, F.J., Davis, M., & Evrard, A. 1995, *ApJ*, 454, 1
- Tormen, G. 1997, *MNRAS*, 290, 411
- Tormen, G., Diaferio, A., Syer, D., 1998, *MNRAS* submitted (astro-ph/9712222)
- van den Bosch, F.C., Lewis, G.F., Lake, G., Stadel, J. 1998, *ApJ*, in press (preprint astro-ph/9811229)
- van Kampen, E. 1995, *MNRAS*, 273, 295
- Viana, P.T.P., & Liddle, A. 1996, *MNRAS*, 281, 323
- White, S.D.M. 1976, *MNRAS*, 177, 717
- Weinberg, M.D. 1994a, *AJ*, 108, 1398
- Weinberg, M.D. 1994b, *AJ*, 108, 1403
- Weinberg, M.D. 1997, *ApJ*, 478, 435
- White, S.D.M., Navarro, J.F., Evrard, A.E., Frenk, C.S. 1993, *Nature*, 366, 429
- Willick, J., Courteau, St., Faber, S., Burstein, D., Dekel, A., & Kolatt, T.S. 1996, *ApJ*, 457, 460
- Zaritsky, D., & White, S.D.M. 1994, *ApJ*, 435, 599